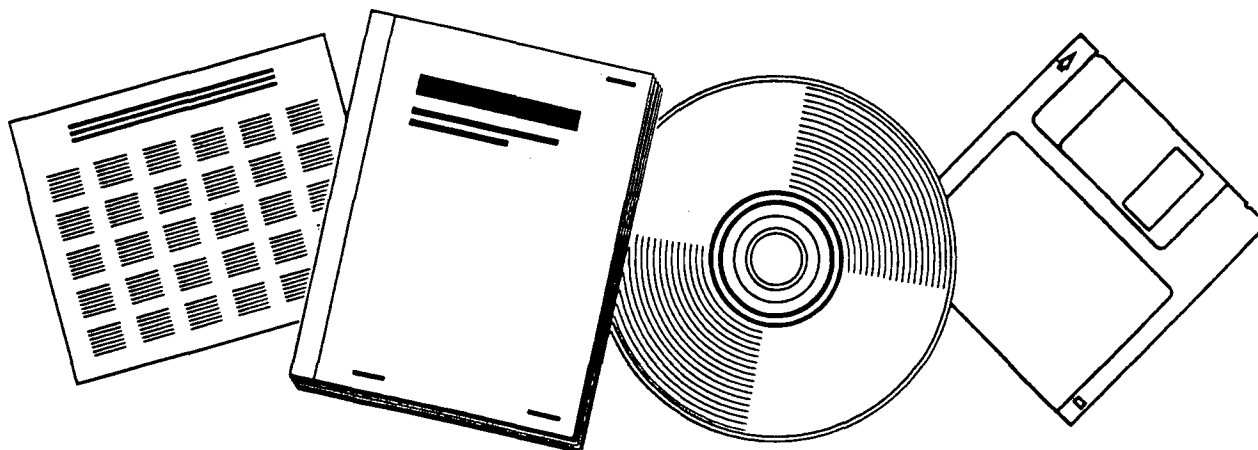**NTIS**

Information is our business.

PAVEMENT PRIMARY RESPONSE TO DYNAMIC LOADING

(U.S.) FEDERAL HIGHWAY ADMINISTRATION, MCLEAN, VA

JUN 97

Pavement Primary Response

To Dynamic Loading

FOREWORD

This report is one of the final reports submitted to the Organisation for Economic Co-operation and Development (OECD) Dynamic Interaction Vehicle-INfrastructure Experiment (DIVINE) project committee by the Federal Highway Administration, Office of Research and Development. The focus of this report is on determining, under controlled test conditions, if the ratio of the dynamic load on the pavement to the strain generated within the pavement varies as the frequency and magnitude of the dynamic load vary.

Results from this report provide useful information to answering many questions regarding the nature and influence of dynamic loading, and the interactions between the vehicle and pavements.

Charles J. Nemmers, Director
Office of Engineering and Highway Operations
Research and Development

NOTICE

1. Report No. FHWA-RD-97-073	PB97-172530	3. Recipient's Catalog No.
4. Title and Subtitle PAVEMENT PRIMARY RESPONSE TO DYNAMIC LOADING		5. Report Date June 1997
		6. Performing Organization Code HNR-30
7. Author(s) William Kenis, David George, Jamel Hammouda		8. Performing Organization Report No.
9. Performing Organization Name and Address Pavement Performance Division, HNR-30 Truck-Pavement Interaction Federal Highway Administration		10. Work Unit No. (TRAIS) 3C4A
		11. Contract or Grant No. In-house Staff Study
12. Sponsoring Agency Name and Address Office of Engineering Research and Development Federal Highway Administration 6300 Georgetown Pike McLean, Virginia 22101-2296		13. Type of Report and Period Covered Final Report October 1994 - March 1997
		14. Sponsoring Agency Code

15. Supplementary Notes
FHWA Contact: William Kenis, HNR-30
In-house staff team members W. Wang, P. Minkel, and D. Fink and the entire DIVINE team especially M. Huhtala, R. Addis, and P. Sweatman are acknowledged for their contributions to this research.

16. Abstract

As part of the Dynamic Interaction Vehicle-INfrastructure Experiment (DIVINE) established in 1992, the U.S. Department of Transportation's Federal Highway Administration agreed to conduct pavement primary response testing to establish how a pavement, and particularly a flexible, asphaltic pavement responds to dynamic loading. The rational being that if the stress and strains generated by dynamically varying loads at critical points in the pavement structure can be measured, then this will help to confirm the benefits of road friendly suspensions.

This research known as Element 2 of the DIVINE project is presented in this report and includes the design, conduct, and findings of the Federal Highway Administration's research. The research performed at the Federal Highway Administration's test road in McLean, VA was conducted on an instumented pavement trafficked by instrumented vehicles. Instantaneous strains generated by the vehicle could be directly related to the instantaneous applied loads and thus an analysis of the primary response due to dynamic loading was undertaken. Furthermore, an artificial plywood bump placed on the test pavement was used to excite different suspension modes. Analysis and results of data are included in this report.

17. Key Words Pavment Primary Response Dynamic Wheel Forces Cross Correlations Dynamic Load Coefficient Dynamic Strain Coefficient	18. Distribution Statement No restrictions. This document is available to the public through the National Technical Information Service, Springfield, Virginia 22161.		
19. Security Classif. (of this report) Unclassified	20. Security Classif. (of this page) Unclassified	21. No. of Pages 66	22. Price

Form DOT F 1700.7 (8-72)   Reproduction of completed page authorized

This form was electronically produced by Elite Federal Forms, Inc.

SI* (MODERN METRIC) CONVERSION FACTORS

APPROXIMATE CONVERSIONS TO SI UNITS

Symbol	When You Know	Multiply By	To Find	Symbol
LENGTH				
in	inches	25.4	millimeters	mm
ft	feet	0.305	meters	m
yd	yards	0.914	meters	m
mi	miles	1.61	kilometers	km
AREA				
in²	square inches	645.2	square millimeters	mm²
ft²	square feet	0.093	square meters	m²
yd²	square yards	0.836	square meters	m²
ac	acres	0.405	hectares	ha
mi²	square miles	2.59	square kilometers	km²
VOLUME				
fl oz	fluid ounces	29.57	milliliters	mL
gal	gallons	3.785	liters	L
ft³	cubic feet	0.028	cubic meters	m³
yd³	cubic yards	0.765	cubic meters	m³

NOTE: Volumes greater than 1000 l shall be shown in m³.

Symbol	When You Know	Multiply By	To Find	Symbol
MASS				
oz	ounces	28.35	grams	g
lb	pounds	0.454	kilograms	kg
T	short tons (2000 lb)	0.907	megagrams (or "metric ton")	Mg (or "t")
TEMPERATURE (exact)				
°F	Fahrenheit temperature	5(F-32)/9 or (F-32)/1.8	Celcius temperature	°C
ILLUMINATION				
fc	foot-candles	10.76	lux	lx
fl	foot-Lamberts	3.426	candela/m²	cd/m²
FORCE and PRESSURE or STRESS				
lbf	poundforce	4.45	newtons	N
lbf/in²	poundforce per square inch	6.89	kilopascals	kPa

APPROXIMATE CONVERSIONS FROM SI UNITS

Symbol	When You Know	Multiply By	To Find	Symbol
LENGTH				
mm	millimeters	0.039	inches	in
m	meters	3.28	feet	ft
m	meters	1.09	yards	yd
km	kilometers	0.621	miles	mi
AREA				
mm²	square millimeters	0.0016	square inches	in²
m²	square meters	10.764	square feet	ft²
m²	square meters	1.195	square yards	yd²
ha	hectares	2.47	acres	ac
km²	square kilometers	0.386	square miles	mi²
VOLUME				
mL	milliliters	0.034	fluid ounces	fl oz
L	liters	0.264	gallons	gal
m³	cubic meters	35.71	cubic feet	ft³
m³	cubic meters	1.307	cubic yards	yd³
MASS				
g	grams	0.035	ounces	oz
kg	kilograms	2.202	pounds	lb
Mg (or "t")	megagrams (or "metric ton")	1.103	short tons (2000 lb)	T
TEMPERATURE (exact)				
°C	Celcius temperature	1.8C + 32	Fahrenheit temperature	°F
ILLUMINATION				
lx	lux	0.0929	foot-candles	fc
cd/m²	candela/m²	0.2919	foot-Lamberts	fl
FORCE and PRESSURE or STRESS				
N	newtons	0.225	poundforce	lbf
kPa	kilopascals	0.145	poundforce per square inch	lbf/in²

* SI is the symbol for the International System of Units. Appropriate rounding should be made to comply with Section 4 of ASTM E380.

(Revised September 1993)

TABLE OF CONTENTS

iii

LIST OF FIGURES

LIST OF TABLES

PAVEMENT PRIMARY RESPONSE TO DYNAMIC LOADING

ELEMENT 2, FINAL REPORT: UNITED STATES RESEARCH

BACKGROUND

Currently, there is worldwide emphasis on improving road freight productivity through the use of higher truck payloads. These higher payloads, have a large potential pay off through reductions in total vehicle operating and transport costs typically representing 10 percent of the Gross National Product. The higher payloads, however, impose higher dynamic loading to pavements and bridges thus having significant impact on the life of the infrastructure and therefore on total infrastructure road costs. Because many of the member countries for the Organisation for Economic Co-operation and Development (OECD) reported that increases in dynamic pavement loading was resulting in increasing rates of road wear, OECD's Road Transport Research Program launched a major 2-year study into the relationship between heavy vehicle dynamic loading and pavement and bridge wear known as the DIVINE (Dynamic Interaction of the Vehicle and INfrastructure Experiment) Project in order to study and to specifically identify the effects of dynamic loading on pavement wear and hence on overall productivity.

Although dynamic loading is the subject of increasing attention, many questions remain regarding the nature and influence of dynamic loading, and the interactions between the vehicle, pavements and bridge. In an attempt to address some of these issues, the objectives of DIVINE were established:

- provide a means for identifying and assessing 'road-friendly' vehicles,

- quantify the improvements in road and bridge life possibly through the use of 'road-friendly' vehicles

- determine whether vehicle and suspension configurations that are 'road-friendly' are also 'bridge-friendly'

The DIVINE project involved more than 20 OECD member countries and included specialists in vehicles, pavements, bridges, road management and transport policy. The project consisted of the following six inter-related research elements:

1.   Accelerated Pavement Dynamic Testing
2.   Pavement Primary Response Testing
3.   Road Simulator Testing
4.   Computer Simulation of Heavy Vehicles
5.   Spatial Repeatability of Dynamic Loads
6.   Bridge Dynamic Loads

Although Element 2 included work conducted by both the U.S. Department of Transportation and the Technical Research Center of Finland, this report presents the design, conduct, and findings of the Element 2 research conducted by the U.S. Department of Transportation and summarizes the overall goals of the Element 2 research proposed by DIVINE. The initial report was critically reviewed by a team of world wide experts in this area and their comments and recommendations have been incorporated into this final report to the fullest extent possible.

OBJECTIVE

The purpose of DIVINE's Element 2 is to determine under controlled test conditions, if the ratio of the dynamic load on the pavement to the strain generated within the pavement varies as the frequency and magnitude of the dynamic load varies. The basic idea of the Element 2 experiments for measuring primary response is to simultaneously measure the vehicle's dynamic wheel forces and the strains within the pavement. The measured dynamic wheel forces are then compared to the measured strains. The rational being: if the strain that is generated at a critical point in the pavement by the dynamically varying load is measureable, then the benefits of road-friendly suspensions, in terms of potential damage to the pavement, can be demonstrated.

INTRODUCTION

Pavement Primary Response is defined herein as the change in existing stress, strain, or deflection at one or more critical points in the pavement due to the application of a loading unit moving across the surface of the pavement. Primary responses are in general complex functions of the pavement structure, the local environment, and the composition and character of the truck traffic on the pavement.

With the inception of DIVINE in 1992, the U.S. Department of Transportation's Federal Highway Administration (FHWA) encouraged OECD to consider primary response testing (similarly as planned for FHWA's Phase II test road experiments) to be part of the DIVINE goals in their study of dynamic effects. Thus, with the establishment of the DIVINE Element 2 program, FHWA agreed to freely share those findings with DIVINE that would be outcomes of a mutually agreed upon FHWA / DIVINE project

The most significant aspect of the overall Element 2 research program is the use of instrumented flexible pavements at two different sites; one being FHWA's instrumented test road and the

other, the Virttaa test site of the Technical Research Center of Finland (VTT). Both sites were instrumented with closely spaced strain gauges so as to track strain movements in the pavement as the test vehicles moved along the pavement's surface. In order to account for the dynamic wheel forces applied to the pavement, all test vehicles had at least one of its axle sets instrumented with strain gauges and accelerometers. Also, in all cases, necessary means were taken so as to keep track of both the lateral and longitudinal positioning of the tires as they passed over the gauges. Another unique feature of the experiments made use of short and/or long plywood bumps placed on the pavement so as to induce dynamic loading through the tires to the pavement as the test vehicle moved over the bump. The long bump was designed to excite vehicle body modes and the short bump designed to excite an axle hop mode.

Because of the important interactive influences between vehicle speed, axle static load levels, material effects (viscoelasticity), suspension type (air versus steel suspension), and lift axle effects on pavement response, FHWA had, prior to DIVINE, planned its Phase II experiments to include these parameters and to employ only a long bump. FHWA's reasoning was that under normal operating conditions of pavement roughness and speed, dynamic wheel loads are dominated by body modes and that the wheel hop mode only becomes significant at higher combinations of roughness and speed. Therefore FHWA had determined for the DIVINE experiments to concentrate testing on the body modes using the long bump and to rely on information obtained from tests at different speeds with and without using the long bump. However, subsequent to these experiments, in November of 1996, FHWA conducted an additional Phase III test series with use of both the short bump and the long bump (the methodology adopted for these Phase III experiments differs somewhat from that used in the Phase II experiments and is considered somewhat superior). The conduct and results of the Phase III tests is were not available at the time of printing this document and they will be published elsewhere.

The purpose of this report is to describe the Phase II (FHWA / DIVINE) experimental work performed and results obtained using FHWA's instrumented test road. All tests and analyses were carried out by FHWA's Truck Pavement Interaction Team (TPI) at the Turner-Fairbank Highway Research Center (TFHRC) in McLean VA. The report includes only those findings associated with tests using the National Research Council of Canada's (NRC) tractor-semi trailer test vehicle with and without the long bump. The report does not include information dealing with lift axles, the FHWA truck (air and steel suspensions), or transverse gauges. Analyses and results pertaining to these effects will be presented elsewhere.

FHWA/DIVINE RESEARCH PROGRAM

The FHWA/DIVINE tests using the NRC truck were conducted in December 1994 using the thick test pavement at the FHWA test road. The major components of the program included:

- Pavement strain measurements
- NRC vehicle equipped with an air suspension system

- Fourth and fifth trailing axles
- Right outside tire of dual tires
- Creep speed and speeds of 15, 25, 35, & 45 km/h
- Vehicle testing under full payload conditions
- Testing performed with and without use of a 3.3 m X 50 mm bump

The overall FHWA test program is given in table 1 along with that portion of the test program that was agreed upon as being mutually FHWA/DIVINE. Also included in table 1 is the overall DIVINE/VTT test program conducted in Finland. For the FHWA/DIVINE test program, the NRC vehicle was run at FHWA using an air suspension at creep speeds and speeds of 15, 25, 35, and 45 km/h, under full and empty payload conditions (only full payload results are reported here), and at a tire pressure of 760 kPa. Pavement strain responses were measured while using the long bump placed on the test pavement to excite different vehicle body modes. Information pertaining to test attributes is presented below.

The Test Pavement

The FHWA Test Road was originally constructed in August 1990 on the access road to the TFHRC located in McLean, VA. It was designed to accommodate 178-mm (7-in) and 89-mm (3.5-in) thick AC pavement test sections each instrumented with several different types of strain gauges and LVDT's. Each test section is 30.4-m (100-ft) long separated by a 7.6-m (25-ft) transition zone. Design plan and cross sectional views of the "thick" section are given in figures 1a and 1b.[1] The thick section was instrumented during construction with 36 in-line H-bar strain gauges placed longitudinally in the outer wheel path, on top of the base course, spaced at 0.3-m (1-ft) intervals in order to study the interactive effects of dynamic wheel force and pavement viscoelastic behavior. The 36 in-line gauges were eventually discarded and replaced with 16 cores as shown in figure 1b. Two phases of testing were planned; Phase I testing was completed in 1991 using all gauges except the 36 in-line H-gauges scheduled for the dynamic tests in Phase II; the Phase I results have been reported elsewhere.[1,2]

Test Pavement Roughness

Both left and right wheel path profiles were acquired using the dipstick over a profiled distance of 304 m that included the 100-m test section used. Test road roughness was calculated in terms of the international road roughness index (IRI). The profile measurements showed that for the left wheel path, IRI= 2.02 mm/m (128.29 in/mile) and for the right wheel path, IRI= 2.10 mm/m (133.27 in/mile). The IRI values indicate that the test road has medium roughness.

---

[1] The 178-mm thickness shown in figure 1a was a target design. The actual thickness of the gauged wheel path section used in this study was 152-mm as determined from the average length of 16 cores taken from the wheel path.

<u>Test</u> <u>Pavement</u> <u>Instrumentation</u>

All of the H-bars installed during construction survived construction, however many of them had deteriorated over the 2 years prior to the DIVINE tests. It was thus determined prior to DIVINE testing not to use the H-bar gauges but instead to retrofit the thick pavement with strain gauged cores manufactured at FHWA. The current installation shown in figure 1 consisted of 16 instrumented (approximate 10.1-cm diameter by 17.8-cm) cores installed in the thick pavements right wheel path and spaced 0.6 m apart on core center for a total length of 9 m. Each of the cores was fitted with four 64-mm long Micro Measurements EA series strain gauges so that when the core was installed in the AC pavement, both top and bottom longitudinal and lateral strains could be measured. Detailed descriptions of the manufacture and installation of the gauges is given in reference (3). Summary of the retrofitting procedure is given below:

- Removed 16, 101-mm diameter asphalt cores from test pavements of FHWA's Accelerated Loading Facility (ALF) using a 108-mm outer diameter bit. The test road pavements were designed identically as the ALF pavements except that the AC ALF mix contained a slightly smaller top size aggregate

- Cored the retrofit locations at the Test Road with a 101.6-mm outer diameter bit and measured the length of each core

- Cut the ALF cores to the length of the Test Road cores minus 1 cm

- Prepared each horizontal surface of the ALF core with epoxy to fill in voids and to provide a waterproofing barrier for strain gauges

- Affixed 57-mm strain gauges longitudinally and transversely to each prepared surface - Cut grooves in pavement to channel instrumentation cable to the shoulder of the Test Road

- Installed the instrumented cores in the test pavement with epoxy

It is important to select an appropriate strain gauge length that is sufficient to bridge over the top size aggregate in the mix so that the measured values will reflect the true strain in the aggregate/binder mix (gauge lengths from 2 to 5 times the maximum aggregate size are considered sufficient). Figure 2 is a diagram of a core fitted with two strain gauges. Since the inplace test road AC surface layer course top size aggregate was 19-mm and the AC binder course top size aggregate 38-mm, a minimum 76-mm strain gauge would be needed. In order to reduce the length of the gauge, the retrofit cores were selected so that the entire core was composed of the identical surface mix course mix containing a 19-mm top size aggregate. The 57-mm strain gauge length selected was thus well within the required gauge length to top size range.

Prior to testing it was determined that 5 of the 16 longitudinal bottom retrofit strain gauges were circumspect only because values from preliminary load testing seemed relatively low. Although

5

these gauges were recorded during testing, measured values were not used in the analysis. In most cases, table entries relating to these gauges are shown as blanks such as in table 6.

The FHWA/DIVINE project limited analyses to the longitudinal top and bottom strain gauges only. The transverse gauges were monitored however the results of analyses of these gauges is presented elsewhere.

Bump Description

Dynamic loading is primarily the result of the two body modes (bounce and pitch) normally occurring between frequencies of 1.0 and 5 Hz, and axle hop, normally occurring between frequencies of 8 and 16 Hz. In general there are as many modes as there are degrees of freedom but in most all cases under normal operating conditions body bounce and pitch dominant. Excitation of the body modes of the vehicle can be achieved through the proper selection of bump geometry and vehicle speed. The OECD DIVINE expert group decided to use only one operating test speed, 45 km/h, and they estimated that use of a 4-m haversine bump (8-m wavelength) at 45 km/h would provide sufficient vehicle body dynamics based on 1.5 Hz body bounce mode at this speed. Had OECD assumed a lower or a higher body mode frequency, say 1 Hz or 2 Hz, then they might have suggested a longer or a shorter length bump more likely in the range of 6-m and 3-m respectively. Had they decided to conduct the experiments at a lower speed they might have also suggested using a slightly shorter length bump. In general, body bounce will be excited through different combinations of speed and bump geometry and since FHWA conducted tests over 5 different speeds with a median 25 km/h speed, a slightly short bump was used so as to obtain decent dynamics at all of the higher speeds.

The FHWA bump displayed in figure 3a was fabricated in FHWA's carpentry shop using 6-mm sheets of plywood laminated together and for the road tests it was bolted to the pavement 30 cm in front of the 1st of the 16 in-line cores. Since the experiment was to be conducted at different speeds, it was therefore important to investigate the influences of the bump length at different vehicle speeds. To do this it was noted that as the vehicle travels over the bump, the excitation from the bump will actually be filtered by the length of the tire in contact with the bump, therefore a 0.3-m moving average filter was applied to approximate the vehicles perception of the bump. The Power Spectral Density of the filtered bump was then computed for the different speeds. These results are presented in figure 3b. The spectra exhibit peaks at frequencies of approximately 1.8, 2.6, and 3.3 Hz at 25, 35, and 45 km/h respectively. Clearly the bump used will provide excitation that are more in tune with body modes between 1.5 and 2 Hz, at a speed of 25 km/h.

The Test Vehicle

Vehicle geometry and individual tire loads under full load conditions are presented in figure 4. FHWA/DIVINE tests were conducted with the NRC vehicle being fully loaded (all water tanks full). With all water tanks of the NRC vehicle empty, the gross vehicle weight (GVW) was 174-kN (39,000-lbf). Under full-load conditions, the GVW was 476-kN (107,000-lbf).

Instrumentation

All wheels on the test vehicle are instrumented with strain gauges and accelerometers at the ends of each axle to measure the dynamic wheel forces. All wheels were monitored, however DIVINE limited analysis to the 4th and 5th axles only. Dynamic wheel forces are obtained by measuring the strains due to shear in the axle between the wheel and the suspension and to correct these for the inertial effects of the outboard mass via an accelerometer. The inertial forces can be calculated using the outboard mass and the acceleration of the outboard mass. Dynamic wheel forces are then obtained by combining the dynamic strain of the axle and the inertial load of the outboard mass of the axle. The outboard mass consists of a portion of the axle, the brake drum, wheel assembly and tires. Figure 5 shows a diagram of the Dynamic wheel force measurement.

Tire Location

Both the longitudinal and lateral position of the tire was accounted for in the experiments. The precise longitudinal location of the wheel force along the pavement was accounted for by the use of an optical sensor attached to the NRC vehicle. As the test vehicle traveled down the test road, the optical sensor detected reflective strips which were strategically placed along the test road. By knowing the distance from the reflective strips to each of the strain gauges, it was possible to match the wheel forces to the corresponding strain response at all strain gauge locations.

Because the strains are sensitive to the lateral position of the passing tire, an exact account of the position of the outside tire with respect to each of the 16 strain gauged cores is required. To do this a series of dots align the test road beginning approximately 100-m before the test section to help the driver properly align the vehicle with the gauges. The lateral position of the tires was monitored by lightly covering the instrumented section with moist sand. Precise lateral distance measurements were recorded at the 2nd, 5th, 10th, and 13th cores. The remaining lateral distance measurements were acquired using linear interpolation.

Data Collection

Considering the number of runs and the time required to view and extract peak strain values from each of the waveforms created by the strain gauges, a computer program called COMPUTE PK, was designed to extract "peak" as well as "valley" strains from all of the 64 strain gauges imbedded in the pavement. Figure 6 shows typical raw strain responses from longitudinal and transverse top and bottom strain gauges as the 5-axle NRC truck passed over the gauge. A second computer program called COMPUTE CAL was developed to calibrate the raw peak strain readings for the three corrective actions, these are: temperature calibration, lateral distance calibration, and variability normalization correction factors. The program outputs the corrected peak strain values after allowing the user to input the raw peak strain values from all strain gauges for one test run, the pavement temperature of the test run, and the vehicle tire lateral distance values.

PRIMARY RESPONSE CALIBRATIONS

Three peak strain calibration actions were conducted to account for variations in pavement temperature from one run to another, variations of lateral position of the tire relative to the core center, and variations in the structural integrity from core to core. These three corrective actions are described in detail below.

Temperature Calibration

All strain responses were adjusted to a standard temperature of 21 °C (70 °F). Temperature within the test section was monitored using a thermistor probe at the top, middle, and bottom of the AC layer. Falling Weight Deflectometer (FWD) calibration tests were conducted over a variety of temperatures throughout the year. For each test, the FWD weight was dropped three times at three different drop heights on to a 30-cm (11.82-in) diametrical load plate positioned directly over the core. The resulting strain in each of the core's four gauges was recorded as well as the peak load applied to the core. This procedure was completed for all 16 cores (64 gauges) on seven different dates (temperature distribution states) from October, 1994 through March, 1995.

Since asphalt concrete is highly sensitive to temperature, it is important to establish the meaning of the term "temperature distribution state" and to have an awareness of what effect different states will have on pavement response. If the temperature is distributed in some fashion $T(t)$ throughout the AC layer thickness (h) such that the temperature at the top $T(top)$ is colder than the temperature at the bottom $T(bot)$ and it is at some intermediate temperature $T2$ at the middle of the layer, then it will strain quite differently under this temperature state than under some other temperature state occurring throughout time. It is difficult to estimate exactly when the same temperature states will exist in a given pavement since such states depend heavily on air temperature history, cloud cover, dew point, etc., thus extrapolating pavement response from a known or unknown random temperature state $T(t)$ to one that is uniformly distributed at 21 °C is precarious at best (such a uniform state may not be existent in nature or it would exist for very short periods of time).

Therefore, it is important to develop a scheme to convert pavement strain response measured at any temperature to a strain response at a standard temperature if comparisons of physical data are to be made. To do this, two different methods of calibration were investigated, a global methodology and a local one. In either case, it was decided to use the temperature $T2$ at mid depth as being representative of the overall pavement cross section. It was reasoned that the pavement will strain depending upon the overall effect of the temperature distribution and not just on the temperature at the bottom or the top. Since the temperature gradients that were measured during the FWD calibration tests were all rather small and linear with depth, on average about 0.22 °C/cm of depth the temperature $T2$ at mid depth was selected the overall temperature of the pavement cross section.

8

Local Calibration

Prior to initiating the global methodology for use in this study, 16 top and 16 bottom temperature calibration curves were developed for each of the 16 top and 16 bottom longitudinal gauges, however it was determined not to use this method as noted. If one were to assume that at the pavement was identical throughout its test length e.g. perfectly uniform materials, layer thicknesses, identical gauge placement and that at some point in time during field testing, the identical pavement temperature distribution existed throughout (not the reference temperature), then shifting the top or bottom responses to the reference temperature using the 16 temperature correction factors, should result in 16 identical strain values, but only if the temperature calibration factors were identical. The acquisition of 16 identical calibration factors would have required all of the calibrations to have been obtained under identical conditions (FWD being consistent throughout) and that the identical temperature distribution pattern existed every time FWD calibration tests were conducted, a somewhat impossible situation--thus the global methodology presented below was developed for use in these experiments. One might also find equally compelling justification for using a local calibration technique however.

Global Calibration

In this method only all that is needed is an average temperature calibration function for each of the four gauge types. Table 2 tabulates the peak longitudinal top strain and peak longitudinal top strain/load ratio calculated for core #0 from FWD tests conducted on October 19, 1994; these data are also shown plotted in figure 7a. Because of the highly linear relationship observed for all similar plots between strain and load at any given temperature, the average of the e/F ratios, M, for all 16 top gauges, can obtained as given in table 3 for the seven different values of T2 (the M ratios highlighted in table 3 are summarized in table 4). To determine the global pavement response of the longitudinal top strain gauges, the M ratios were plotted versus the corresponding seven mid pavement temperatures T2 as shown in figure 7b along with the linear regression line ($R^2 = 0.97$). The equation for the Longitudinal top gauges is

$$M(T2) = m \cdot T2 + b \qquad (1)$$

where $\qquad b = -1.9226500$

$\qquad m = -0.1351256$

For any run, the corrected peak strain e_{21} at 21 °C (70 °F) is obtained for each longitudinal top gauge at any temperature T2 by dividing the measured peak strain e_{21} by a correction factor CF_{21} defined as

$$CF_{21} = M(T2)/M(21) \qquad (2)$$

where M(21) = -4.77530 and M(T2) is determined from equation (1) for each run. This process

was followed for the bottom longitudinal and lateral gauges similarly.

Lateral Distance Calibration

Because pavement strains are sensitive to the lateral position of the passing vehicle tire, a lateral distance calibration was developed to correct all recorded strain readings as if the center of the vehicle tire passed directly over the strain gauge during testing. The method involved the conduct of numerous creep speed test runs recording the lateral position of the 5th axle outside right rear tire with respect to each of the 16 cores embedded in the wheel path and the peak strain of all 64 gauges while the NRC vehicle passed over the strain gauges at various lateral positions. Because the tire width is 21 cm, the lateral distance measure of -10.5 cm is when the center of the outside tire is directly over the strain gauge. The steps emanating from this process are demonstrated in table 5a for the longitudinal top gauge of core 7. The first step is to correct all measured peak strains to standard strains, 21 °C (70 °F), as shown in table 5a (column F). The temperature corrected strains were then plotted against the corresponding measured lateral distances (column C) as shown in figure 8. From these results, a best fit curve is obtained by regression analysis in accordance with the equation

$$Y(X) = A(X^6)+B(X^5)+C(X^4)+D(X^3)+E(X^2)+F(X)+G \qquad (3)$$

where the dependent variable $Y(X)$ is longitudinal creep strain for core 7 and the independent variable X is the lateral distance mentioned above (the highlighted values at the bottom of figure 8 are the constants A through G resulting from the regression analysis performed on the curve in figure 8).

The temperature and lateral distance calibrated strain $e_{21,-10.5}$ for any other test run, at any speed, at lateral distance X (top strain at core 7) is obtained by dividing the temperature corrected peak strain, $e_{21,X}$ for that test run by the lateral distance correction factor CF_X defined as

$$CF_X = Y(X) / Y(-10.5)$$

where $Y(X)$ is obtained from equation 3 for that test run and lateral distance offset and $Y(-10.5)$ is the correction factor normalizing constant as shown calculated in table 6 for longitudinal top gauge at core 7 (note, there are 64 $Y(-10.5)$ constants each associated with each of the 64 gauges). In the example of core 7, $Y(-10.5)$ equals -521.69 microstrain. Column F table 5b shows the value of the lateral distance normalization factor CF_X. Finally, column G table 5b shows the temperature and lateral distance normalized strains.

All parameters for all transverse and longitudinal top and bottom linear regression curves are included in the COMPUTE CAL program thereby when inputting the vehicle lateral distance of a test run, the strain of all longitudinal top and bottom gauges are normalized for lateral distance. The method assumes that lateral distance calibration is independent of temperature.

Variability Calibrations

Because of the heterogeneous nature of the material properties and/or thickness and density variations of the layers, structural integrity will vary from one point in the pavement to another. Additionally, since the strain gauges are glued to AC materials, then their responses will be dependent on the degree of heterogeneity of the AC material, on the uniformity of gauge-AC contact, and in this particular case, on the uniformity of contact between the AC core and pavement. Because of these variabilities, the strain gauges must be calibrated to correct for these differences in the structural variability from gauge to gauge. This was accomplished as follows:

- Peak strains from the creep tests were first corrected for temperature and lateral distance.
- All 16 longitudinal surface gauges were normalized to each other by dividing each longitudinal gauge's peak strain value at -10.5 cm by the average of all longitudinal peak strain values at -10.5 cm. The resulting value is called the "variability normalization factor " CF_V (see table 6).

This above process was performed for all longitudinal as well as transverse top and bottom gauges.

DATA VIABILITY

The viability of the measured data was assessed in terms of

- significance of calibrations
- repeatability of wheel force and strain on repeat runs
- peak strains and wheel forces
- peak strain magnitude

A series of correlations and cross correlations were conducted in an attempt to better understand the validity and meaning of the measured data. In evaluation of what follows, the reader should be aware that in these analyses a correlation coefficient of 1 means perfect linearity between the two variables and that the ocurrance of the independent variable can be explained entirely by the actions of the dependent variable. A high positive correlation of say 90 percent means that approximately 90 percent of the occurrence of the dependent variable can be explained by the independent variable but that 10 percent of the occurence of the independent variable must be due to some other action(s).

Significance of Calibrations

Peak strains for one test run at each of the 16 gauge locations are plotted at each of the three stages of calibration in figure 9 for the 5th axle. The four graphs shown represent plots of the wheel forces versus the following strain responses:

11

- Uncalibrated strain response
- Strain response calibrated for temperature
- Strain response calibrated for temperature and lateral distance
- Strain response calibrated for temperature, lateral distance, and structural variability

It is seen in figure 9 that temperature calibration has caused a uniform upward shift of all the data points, the lateral distance calibration very slight improvement, and significant improvement when structural variability calibrations are applied.

Because the same temperature correction factor is applied to each of the 16 top or bottom gauges in a given run, then correlations for that run between load and peak strain should not be effected as is the case as shown in figure 10. This figure compares correlation coefficients calculated from correlations conducted between peak strain and wheel force after each stage of calibration for the 4th axle using the bump at a speed of 45 km/h. Since the truck runs at approximately the same offset distance from each of the gauges in a given run, it is expected that correlations between peak strain and load will be effected only very slightly for that run as is the case shown in the figure. The importance of the structural variability calibrations is depicted in figure 10 increasing the correlation coefficient by 80 percent thus emphasizing the significance of the major influencing effects on structural variability: material, geometric and gauge placement.

Repeatability of Wheel Forces and Strain on Repeat Runs

Correlation coefficients between the peak wheel force occurring at each of the 16 gauges on a given run (with bump) at 45 km/h and the wheel force occurring on some other run (with bump) at 45 km/h are plotted in figure 11a. Given that all correlation coefficients are above 0.9, it is sufficient to say that almost identical wheel force data (high level of force spacial repeatability) is obtained on repeat runs with use of the bump at 45 km/h.

Correlation coefficients between peak strain occurring at each of the 16 gauges on a given run (with bump) at 45 km/h and peak strain occurring on some other run are plotted in figure 11b. Given that all correlation coefficients are above 0.9, it is sufficient to say that almost identical peak strain data (high level of strain spatial repeatability) is obtained on repeat runs with the use of the bump at 45 km/h. Similar findings were obtained at other speeds for both the 4th and 5th axles with use of the bump. Without the bump, coefficients were only slightly lower.

Cross Correlations Between Peak Strains and Wheel Forces

For a given run, cross correlations between wheel force and peak strain, for the 4th and 5th axles at the four speeds with and without use of the bump were conducted. Correlation coefficients are generally above 0.9 with use of the bump at all speeds as seen in figure 12. The high positive correlation means that about 90 percent of the peak strains can be explained by wheel force when the bump is used. A high correlation coefficient also means that there is a high degree of linearity between the two variables being correlated.

12

For the 4th an 5th axles without use of the bump, there is little or no correlation between load and strain except at 45 km/h where the correlation coefficient is around 0.70. The better correlations at 45 km/h are best explained by the higher signal to noise ratios due to increased dynamics. Consequently at normal highway speeds where the dynamics are expected to be even higher, we would expect increasingly better correlations possibly approaching those obtained using the bump.

Strain Levels

A rough idea as to the validity of the levels of strain measured in the pavement can be obtained through the use of a elastic multilayer theory computer program. A recent version of VESYS which includes an improved elastic layer code to calculate pavement primary response was used. The rear right half tandem axle geometry and loads as shown in figure 4b were used in the program. The following pavement input parameters were also used:

Layer 1 - Asphalt concrete: E=1379 kPa (200,000 psi), μ=0.35
Layer 2 - Base course: E= 138 kPa (20,000 psi), h=30.5 cm (12.0 in), μ= 0.4
Layer 3 - Subgrade: E= 35 kPa (5,000 psi), μ= 0.4

AC layer thicknesses were obtained from postmortem coring data at the location of the strain gauges as shown in table 7 (measured AC layer mean thickness was 15.2 cm (6") with coefficient of variation of 5 percent). The actual strain gauge location for each core and the theoretical calculation results are also listed. The strains shown were calculated under the center of the outer tire of the 5th axle at the depths where the strain gauges were located.

Since all installed strain gauge cores were 14 cm long, most top strain gauges were located below the surrounding pavement surface and some bottom strain gauges below the bottom of the surrounding AC layer. The results tabulated are evidence that bottom tensile strain should be between 46 and 92 percent smaller than top strain. These calculations are completely in line with test measurements.

ANALYSIS OF DATA

Analyses of data are presented below in terms of

- dynamic wheel forces
- primary responses
- viscoelastic effects

Dynamic Wheel Forces

In order to study the form of the dynamic loading on the test pavement two types of analyses were performed, a spectral analysis and calculation of the dynamic load coefficient (DLC).

Analyses and significance of these data are presented below.

Spectral Analysis of Wheel Force Data

Any periodic signal may be represented by a series of sine wave functions at different amplitudes, frequencies, and phase shifts which when summed together for each series increment will reproduce the original signal. The frequency content of a periodic signal may be obtained by taking its Fast Fourier Transform (FFT). For a random signal (non periodic) the FFT of the signal does not exist but the FFT of its autocorrelation function does exist. Because the autocorrelation function has the property of preserving the frequency content of the signal, we can take the FFT of the autocorrelation function called the Power Spectral Density (PSD) to obtain the frequency content of the original signal.[4] All calculations of PSD were obtained from data points representing the entire trace of the wheel force over an 80-m length including the bump where appropriate.

Plots of the PSD for the 4th axle's wheel force data with and without the bump are given in figures 13a and 13b respectively for 15, 25, 35, and 45 km/h. The dominant frequencies at the higher speeds (25, 35, 45 km/h) using the bump are evidenced at 1.5 Hz. The dominant frequencies at these speeds without the bump occur between 0.5 and 1.5 Hz; we assume these frequencies with and without the bump to represent body mode frequencies. The effect of using the bump at the higher speeds is quite obvious noting that the powers of the body mode frequencies using the bump are between 10 and 40 times greater than not using the bump. It is interesting to note from these figures that maximum body mode dynamics are attained at the 25 km/h with use of the bump supporting earlier notations that the 3.3-m bump will influence body modes more at the 25 km/h speed. Results for the fifth axle are about the same as those found for the fourth axle thus this information will not be repeated here. [2]

Dynamic Load Coefficient

The dynamic load coefficient (DLC) of the wheel force data is a statistical measure reflecting tire force deviation from a mean value. It is defined statistically as the standard deviation of the wheel force data divided by the average of the wheel force data and it is thus identical to the coefficient of variation. One should also note that the DLC is a measure of the area under the PSD plot. All calculations of DLC when referenced to top strain gauges were obtained using the wheel force as it was measured directly above one of the 16 in place longitudinal strain gauges. Since 8 of the 16 bottom gauges were considered circumspect, all calculations of DLC when referenced to bottom strain gauges were obtained using the wheel force as it was measured directly above only 8 of the bottom gauges.

---

[2] There is evidence of the wheel hop, at the higher speeds between 11 and 12 Hz but at very low power. At creep speed peak PSD's are 7 to 10 times greater with use of the bump than without use of the bump possibly reflecting the natural frequency of the tire.

14

The DLC's computed for the 4th and 5th axle of each test run are plotted in figure 14. It is seen that the DLC's for the 4th and 5th axles are quite similar and the highest DLC's occur using the bump at the higher speeds, 25, 35, and 45 km/h. It is also seen at the higher speeds, that the DLC's measured for both axles using the bump are roughly 3 to 10 times greater than those measured not using the bump. It is seen that the DLC's are equally high at 25, 35 and 45 km/h indicating that the bump is the major contributor to these fluctuations. Note that at 25 km/h, the PSD is higher & narrower dictating that the bump at 25 km/h provides excitations that are more in line with the body mode of the truck at that speed, but the wider and lower PSD's at 35 and 45 km/h are evidence support the occurrence of equally high DLC's at these speeds.

When the bump is not used, the DLC's seem to increase more gradually and they are greatest at 35 and 45 km/h. The assortment of wave lengths in the pavement have therefore excited the body bounce mode at each of the test speeds in a similar fashion. We would expect that the DLC's would increase to some point with speed however we did not run the vehicle beyond the 45 km/h speed (we did however run the FHWA vehicle up to 75 km/h and will report on this later).

Primary Response

Longitudinal top and bottom strain occurring under the center of the outside rear tire (right side) from each of the 16 cores were recorded at 45, 35, 25, 15 km/h and at creep speed, with and without use of the bump.

Wheel Force and Strain Traces

In figures 15a and 15b, top and bottom peak strains along with wheel force are plotted versus distance, with and without using the bump, for selected test runs at creep speed, 15, 25, and 45 km/h. It is clear that with use of the bump, both bottom and top strains seem to track the dynamic loads reasonably well. With use of the bump at the higher speeds, the force trace shows evidence of the 1.5 Hz body frequency as does the strain trace. There is some evidence that the force trace shows wheel hop between 12.5 and 16 Hz but the strain response to this excitation is not so distinguishable.

Without the bump, body frequency and strain are not distinguishable. Although wheel hop frequency is somewhat visable as above, the induced strain is indistinguishable. It is also clear from figure 15 that bottom strains are lower than top strains as discussed later under "Strain Levels".

General Load-Strain Statistics

General statistics pertaining to wheel forces and peak strains over all test runs with and without the bump and at each speed are given in tables 8a through 8h. Observations drawn from these data are :

(a) Both with and without the bump for all speeds, the average of the mean dynamic load for the 4th axle (5th axle) ranges between 59.7 and 61.4 kN (60.3 and 62.1 kN). Since the static wheel load for the 4th axle (5th axle) is 60.3 kN (61.3 kN) we see that mean dynamic loading is very close to the static load (independent of speed and whether or not a bump is used). Since convergence to the static load is related to the number of points sampled, this is sufficient justification that the sample (16 points) was large enough to capture all characteristics of the load. (The fact that the desired body modes were identified, supports the selection of a 0.6-m gauge spacing for body bounce).

(b) At the higher speeds (25, 35, and 45 km/hr) without the bump, the average of the maximum bottom strains for the 4th axle (5th axle) is about 55 percent (52 percent) less than the average of the maximum top strains. With the bump, the average of the maximum bottom strains is 58 percent (54 percent) less than at the surface for the 4th and 5th axles respectively. Similarly without use of the bump, the average of the mean bottom strains for the 4th axle (5th axle), is 56 percent (55 percent) less than the average of the mean top strains and 55 percent (58 percent) less with use of the bump. A theoretical basis for these findings is given in the section "Strain Levels".

(c) The average of the mean strain is in all cases slightly less (3 to 9 percent) with the bump than without the bump. One possible reason is that the bump is placed within 10-cm of the first gauge and as the wheels of the vehicle pass over the bump the wheel forces are dispersed so that the gauges close to the bump sees virtually zero strain as the wheel is on the bump e.g., gauges close to the bump may not have experienced the same time of loading as the gauges further down line experienced.

(d) The bump as compared to no bump has caused the average maximum dynamic load for the 4th axle (5th axle) to increase 21 percent (24.5 percent) and average maximum top strain for the 4th axle (5th axle) to increase 5.7 percent (12.6 percent). For the bottom strains for the 4th axle (5th axle), the bump caused the maximum dynamic load (using only 8 points) to increase by 17 percent (20 percent) and maximum strain by 1 percent (5 percent).

(e) Using the bump, the maximum dynamic load under the 4th axle (5th axle) is 32.6 percent (32.1 percent) greater than the mean load and the maximum top strain is 32.9 percent (31.2 percent) greater than mean top strain. The maximum load under the 4th axle (5th axle) is (using only 8 points) 23.9 percent (30.8 percent) greater than the mean load while maximum bottom strain is 23.8 percent (33.3 percent) greater than the mean bottom strain using the bump. This observation suggests linearity.

(f) For the 4th axle (5th axle) without use of the bump, the maximum load is 7.9 percent (8.2 percent) greater than mean load and maximum top strain is 12 percent (17 percent) greater than mean top strain. For the bottom gauges maximum load for the 4th axle (5th axle) is 5 percent (7 percent) greater than mean load while maximum bottom strain is 12 percent (17 percent) greater than mean bottom strain not using the bump. This observation also suggests linearity.

Regressions

Peak pavement strains occurring on each run and each gauge versus the forces that occur directly above the gauge are plotted in figures 16a through 16d for the higher speeds only. Linear regression of the points was performed to determine the degree of a linear relationship shown in the figure. The latter two columns in table 8 are results from linear regression analysis yielding the R^2 and the resulting slopes of the linear regressed curves. The R^2 is a measure of the variation of the data points from the linear line and thus has similar interpretation to the correlation coefficient discussed previously under Data Viability. If the intercept in the linear fit is computed rather than being forced to be zero, then R is equal to the correlation coefficient. The R^2 value is only given in the figure if it is greater than 0.5 to suggest that strain might possibly be explained by wheel force. The slopes of the linear lines were computed, only if the R^2 was found to be greater than 0.6.

The following observations are made from table 8 and from figure 16:

(a) Good correlations for top and bottom gauges using the bump were obtained over a rather wide range in dynamic wheel forces, attributable primarily to the different speeds used. This means that a linear relationship between load and top or bottom strain can be expected to exist and will certainly allow one to estimate pavement response with greater confidence. The bump causes the body modes to be emphasized as was discussed previously under the section on PSD and DLC. The range in loads experienced for the 4th axle (5th axle) is between 60 and 142 percent of the static wheel load of 61.3 kN (between 66 and 140 percent of the static wheel load of 60.3 kN).

(b) Correlation is poor without using the bump because of the broader band of excitations and smaller amplitudes. The lower correlations then could be a result of the gauges in the pavement not being able to pick up the high frequencies while the truck instrumentation does and also because of the high noise to signal ratio present under these conditions.

(c) For a given load, surface strains are somewhat higher than bottom strains.

(d) The linear line slopes of the top gauges in figures 16a and 16b are about 2.5 times greater than the slopes of the bottom gauges. If these slopes are considered as a measure of pavement compliance (inverse of stiffness) to loading then the surface of the pavement is more compliant, thus, the surface would deform or stretch more readily than the bottom. This is understandable considering that the surface is confined by stress only in half space while the bottom is confined by stress in full space.

(e) The slopes of the regressed lines are quite similar for the 4th and 5th axles.

17

The Dynamic Strain Coefficient DSC

The term Dynamic Strain Coefficient, DSC is introduced in this report and defined as the standard deviation of the strain data divided by the average of the strain data. The DLC's and DSC's are compared in figures 17a through 17d. Note that with the bump and at the higher speeds, the DSC tends to follow the DLC (suggesting linearity) but at the slower speeds and especially for the bottom gauges there is greater disparity mostly due to the viscoelastic influences of the pavement. Note also that dynamic variations are considerably greater with the bump and that with the bump these statistics are highest between 25 and 45 km/h. Without the bump the DSC is in most cases greater than the DLC. This loss of linearity in absence of the bump is mainly due to signal to noise ratio. When the amplitude is large (bump), the errors that accumulate (due to calibrations, measurement of load, etc.) become less important and do not affect the DLC, DSC relationship significantly. In absence of the bump, errors become significant because of the small measurements being analyzed.

Dynamical Effects on Linearity

If we define an increment in dynamic loading about the mean load $\overline{P}$ as:

$$d\overline{P} = \overline{P} * DLC$$

then the increment in dynamic strain about the mean strain is

$$d\overline{e} = \overline{e} * DSC$$

For a linear system which may be either an elastic or viscoelastic system, the dynamic strain increment must be proportional to the increment in dynamic loading through a proportionality factor. This definition of linearity then mandates that the DLC be identical to the DSC. Deviations from unity can then be considered as one measure of the degree of nonlinearity of the pavement wherein a value of one indicates complete linearity.

A clearer picture of these nonlinearity are obtained by plotting the ratio DSC/ DLC as shown in figures 18a and 18b.   At the lower speeds with or with out the bump, the ratios deviate considerably from unity and are in all cases greater than unity suggesting deviations from linear elasticity (not from linear viscoelasticity). In these cases a small dynamic load increment has caused a large strain increment and this is attributable to the viscoelastic effects of the pavement at long loading times.

At the higher speeds the ratio of DSC to DLC quickly approaches and remains close to unity. The system therefore approaches a linear elastic system somewhere between 15 and 25 km/h

with the bump and between 25 and 35 km/h without the bump. From these plots it is sufficient to speculate that the viscoelastic nature of the pavement has caused the strain to increase because of the longer loading times.[3]

Viscoelasticity and Dynamic Loading Effects

In order to distinguish between pavement viscoelastic behavior and dynamic loading effects, it was imperative that the experiment cover a range of speeds from creep speed wherein viscoelastic effects are greatest to considerably higher speeds wherein all viscoelastic behavior becomes negligible. The speed wherein viscoelastic effects become negligible is defined herein as the viscoelastic-elastic (VE-E) transition speed. The VE-E transition speed however is highly dependent on pavement temperature e.g., under very cold temperatures the AC pavement layer will respond completely elastically at the glass transition temperature usually around minus 12°C (10°F) and mean strain will be totally independent of vehicle speed. However at higher temperatures the pavement will deform continuously under static loading depending upon the length of time the load is actually applied to the pavement. Thus a rapidly moving constant load on the pavement will cause less strain in the pavement than will a slowly moving constant load. The phenomenon of viscoelasticity has just the opposite effect from what one might expect from a dynamic tire load moving over a linear elastic pavement. In this case, the oscillating moving force will impart to the pavement a strain which is linearly proportional to the moving force. The problem is then to identify which of these effects are greater, how to minimize these effects and how to account for them in the practical applications of pavement design and truck size and weight regulations.

In order to investigate these interacting effects, normalized mean strains were plotted versus speed for the 4th and 5th axles and top and bottom gauges as seen in figures 19a and 19b.[4] The most striking feature of these curves is the large increase in mean strain that occurred at slow vehicle speed. For the 4th axle (5th axle) without the bump, average mean unit top strain is increased 71 percent (53.7 percent) due to reducing speed from 45 km/h to creep speed. The increase in average unit mean bottom strain due to the viscoelastic effects for a similar speed reduction is 53 percent (41 percent) for the 4th and 5th axles respectively. The VE-E transition speed is observed to be around 25 km/h and thus viscoelastic behavior will have substantially disappeared at speeds beyond 25 km/h. The pavement may then be considered as being independent of speed at speeds beyond 25 km/h. This finding together with the finding of linearity depicted in figures 16a and 16b are sufficient to establish that the pavement is truly linear elastic at all speeds beyond 25 km/h.

_____

[3] The smaller deviations from unity that occur without using the bump at the higher speeds could be due to other nonlinearities or most likely due to errors in measurement.

[4] The normalized mean strain for a given run is the ratio of the average of the mean strain of all gauges divided by the average of the mean wheel force.

From a practical perspective, assuming that the dynamic load at any point spatially along the pavement has a Gaussian distribution and that the relationship between load and strain is linear, then the following statistics are of interest: mean strain plus 1, 1.645, and 3 standard deviation limits (sigma), representing 84th, 95th, and 99.8th percentile strains. The second statistic was adopted by previous studies [5,6] based on the assumption that damage (or loss of serviceability) due to dynamic loading is caused primarily by the highest loads. The third statistic is an approximation of the maximum dynamic strain that will have occurred spatially under any given moving dynamic load. These statistics at the different testing speeds are plotted in figure 20. It is seen in figure 20 for the test speeds considered, that the viscoelastic strains (425.5 microstrain top and 173.9 microstrain bottom) are appreciably higher than the mean elastic strains (247.2 microstrain top and 111.9 microstrain bottom) and as well, the maximum dynamic elastic strain (mean elastic strain plus three standard deviations). It is however important to note that highway speeds are generally around 100 km/h and consequently the dynamic strain response will be higher than those measured at 45 km/h.

A methodology is presented below to estimate the critical strain in the pavement (either elastic or viscoelastic) based upon a knowledge of the bounds of the maximum attainable pavement strain under any given set of conditions of road roughness and vehicle speed. The methodology described was taken from technical documents after [7]. The assumptions basic to the methodology are:

- The distribution of tire load is Gaussian.
- The tire does not leave the ground for all conditions of roughness and speed of interest.
- There is a linear relation between tire load and pavement strain.
- Pavement structure is homogeneous (no variability).

The first assumption is widely accepted; the second assumption is normally true except for walking beam suspensions at high roughness and high speed. The third assumption is supported by the current study. The last assumption is made for simplicity. Figure 21 provides a summary of the methodology.

From the first assumption it follows that the distribution of loads is symmetric with respect to the mean. The second assumption combined with the first implies that the minimum tire load is zero and the maximum is twice the mean. The third assumption of linearity implies that maximum dynamic strain is twice the mean strain:

$$e_{E_{max}} = 2\,\bar{e}_E$$

20

where $\bar{e}_E$ is the mean elastic strain and $e_{E_{max}}$ is the maximum dynamic elastic strain.

The maximum attainable standard deviation, σ_{max} under any condition of roughness and speed is

$$\sigma_{max} \simeq \frac{\bar{e}_E}{3}$$

The maximum attainable 84th an 95th percentile elastic dynamic strains are defined as

$$e_{84th_{max}} \simeq \bar{e}_E + \sigma_{max} = \frac{4}{3}\bar{e}_E$$

$$e_{95th_{max}} \simeq \bar{e}_E + 1.645\,\sigma_{max} = \frac{4.645}{3}\bar{e}_E$$

For the 4th axle test results, the maximum attainable 84th and 95th percentile elastic dynamic strains are 329.6 and 382.7 microstrains for the top and 149.2 and 173.26 for the bottom gauges respectively. Note that these strains are lower than the viscoelastic strains of 425.5 microstrain and 173.9 strain for the top and bottom gages respectively.

The factor H_m shown in the figure is defined as

$$H_m = 3\left(\frac{e_v}{e_E} - 1\right)$$

where e_v is the viscoelastic strain measured at creep speed, and the subscript m stands for a measured value. The probability (R_{Hm}) that the dynamic strain will not exceed the viscoelastic

21

strain is

$$R_{H_m} = 0.5 + \frac{1}{\sqrt{2\pi}} \int_0^{H_m} e^{-\frac{1}{2}z^2} dz$$

For $H_m = 0$ the pavement behaves elastically and the probability that the dynamic elastic strain is less or equal to the mean elastic strain is 0.5. For $H_m = 1$; 1.645 the associated R_{Hm} values of 0.84 and 0.95 indicate that 84%, and 95% of the elastic dynamic strains will be less than the viscoelastic strain.

If R_{Hm} is viewed as a reliability measure, then H_m as determined from experiment can be used to determine the critical strain for a desired reliability R_{hd} (H_d) that xx percent of strain will not exceed a prescribed value

$$e_d = \bar{e}_E (1 + \frac{H_d}{3})$$

If $H_m > H_d$ then the critical strain is e_v; if $H_m < H_d$ then the critical strain is e_d and if $H_m = H_d$ then $e_v = e_d$. For the 4th axle $H_m = 2.164$ for top strain and 1.662 for bottom strain and the R_{Hm} values become 0.982 and 0.952 for top and bottom respectively. Stated differently, 98.2 percent of all dynamic strain responses at the top will be less than the viscoelastic (creep) response and 95.2 percent of all dynamic strain responses at the bottom will be less than the viscoelastic response.

Since higher temperatures and also thicker AC layers tend to accentuate viscoelastic effects, then the critical strains are most likely to be set by e_v, especially in the hotter regions. For the colder regions and thinner pavements it is likely that the critical strains would be set by dynamic effects. The conduct of dynamic field experiments similar to those conducted for this study will of course be required but they can be accomplished with greater efficiency. The use of bumps will not be necessary and since H_m depends only on mean strain (viscoelastic and mean elastic), these data will be achievable with improved accuracy due to the cancellation of dynamic measurement errors. It is suggested that three or four different test sites be considered in different climatic regions and that two to three different AC layer thicknesses be included in each test site. Although the concept presented refers specifically to pavement strain, it would be equally applicable to other measures of pavement primary response such as deflection or stress.
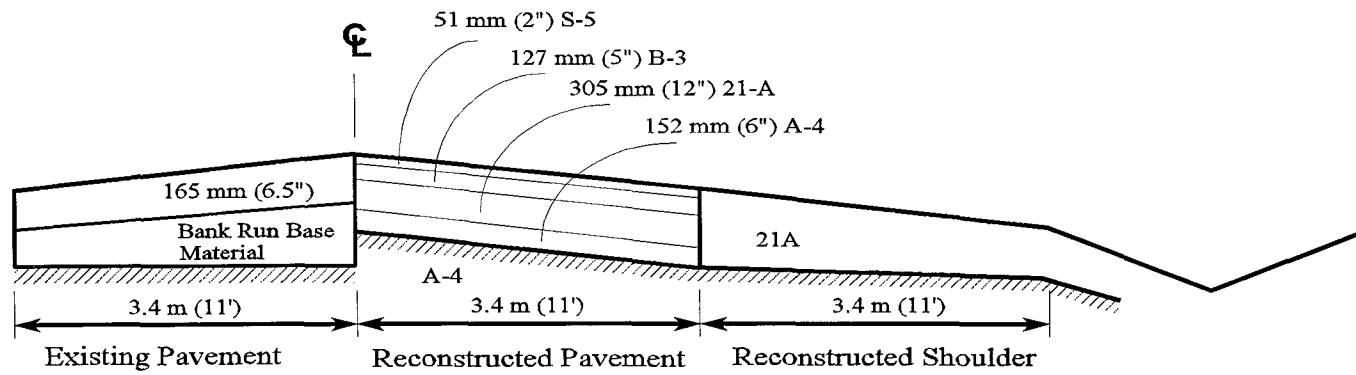
CONCLUSIONS

There were many findings that emanated from this research activity, some supporting previous research and or thoughts and some that may tend to provoke additional thought and experiment. All of the findings presented here relate to a light to medium strength AC pavement with nominal AC layer thickness of 152-mm overlying a 127-mm crush stone base course. All pavement strain data are transposed to a standard temperature of 21 °C. The findings are related to wheel force as it is measured on the axle and to the strain in the pavement that occurs under the outside tire of the dual tire set. The dynamics are induced to the pavement through a combination of different speed levels, use of a prefabricated bump and through the natural roughness of the test pavement having an IRI of 2.2 mm/m. The findings, not in order of importance are presented below.

1. For the higher vehicle speeds studied (speeds between 25 and 45 km/h), a linear elastic relationship was found to exist between dynamic wheel force and the horizontal tensile strain occurring both at the bottom and at the top of the AC layer. The slopes of strain versus load for the top gauges are between 3 and 4 μe/kN and for the bottom gauges between 1.4 and 1.8 μe/kN. The slopes are not appreciably affected by speed changes between 25 and to 45 km/h. It is anticipated that this condition will continue to exist for vehicle speeds higher than those studied in these experiments.

2. Because a flexible pavement system is essentially viscoelastic, its response will be increased for slowly moving loads. Although the pavement responds linearly elastically at the higher speeds, a large increase in mean pavement strain is observed because of the viscoelastic material behavior of the pavement under test vehicle traffic moving at low or creep speed. At normal road roughness conditions, average mean unit strain at the top of the pavement is increased between 50 and 70 percent and bottom strain is increased between 40 and 55 percent when vehicle speed is reduced from the average high test speed (25 to 45 km/h) to creep speed.

3. The mean dynamic load is very close to the static load and was found to be independent of speed and whether or not a bump is used.

4. The average of the maximum bottom strain is between 52 percent and 58 percent less than top maximum strain with or without use of the bump. The average of the mean bottom strains are between 55 percent and 58 percent less than mean top strain. A precise multilayer analysis using the latest version of VESYS conclusively supports these measurements.

5. Without use of the bump for the 4th axle, the maximum load is 7.9 percent greater than mean load and maximum top strain is 12 percent greater than mean top strain but with the bump the maximum load is 32.6 percent greater than the mean load and the maximum strain is 32.9 percent greater than the mean strain.

6. The results of this experiment indicate that meaningful conclusions can not be derived from use of one gauge for any experiment where speed is a parameter due to the large variability range of the strain reading and its speed dependency. Assuming the strain response to be Gaussian, the variability in the reading of a gauge could be as high as plus or minus 15 percent, and plus or minus 75 percent for DSC of 0.05 and 0.25 respectively. These errors are not eliminated by averaging multiple runs, due to the high repeatability of the measurement for a given speed.

7. In order to determine the significance of dynamic loading as it relates to pavement design, a new concept is introduced based on the different representations of pavement loading. The concept demonstrates that pavement design should not be based on mean dynamic loading (static loading) since critical response values are achieved either at creep speed or at high speed. The new concept accounts for type of traffic, speed, and desired reliability. Recommendations are made for the conduct of experiments to determine the critical elastic or viscoelastic response.

51 mm (2") S-5

127 mm (5") B-3

305 mm (12") 21-A

152 mm (6") A-4

165 mm (6.5")

Bank Run Base
Material

21A

A-4

3.4 m (11')

3.4 m (11')

3.4 m (11')

Existing Pavement

Reconstructed Pavement

Reconstructed Shoulder

S-5: Asphalt concrete, typical dense grade, max. agg. 12.5 mm
B-3: Asphalt concrete, typical dense grade, max. agg. 37.5 mm
21-A: Crashed aggregate base, dense graded
A-4: Subgrade soil, nonplastic, silty sand

Figure 1a. Cross Section of Test Road
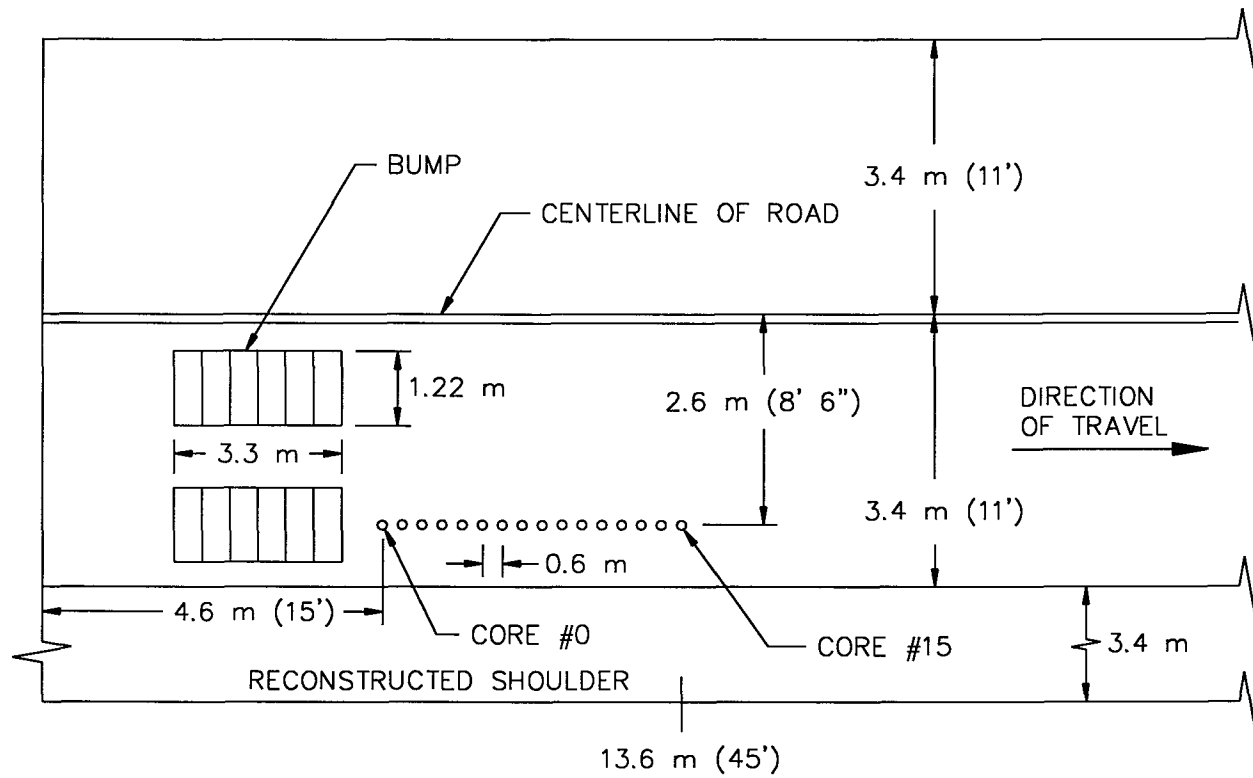
Figure 1b.   Plan View of Test Pavement
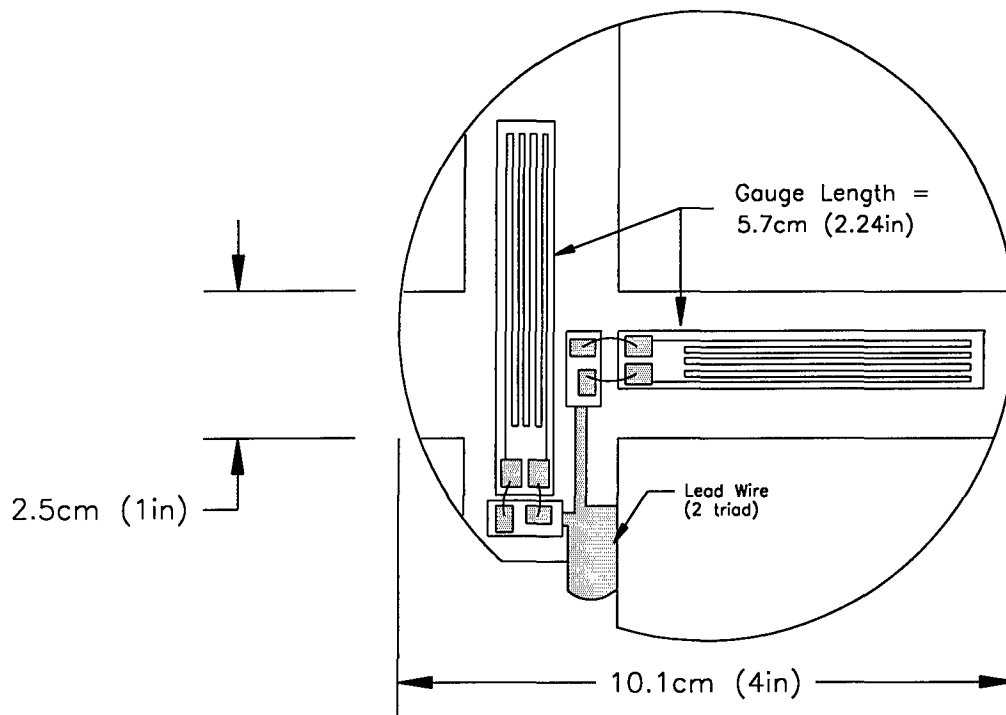
Figure 2a. Plan View of Instrumented Core
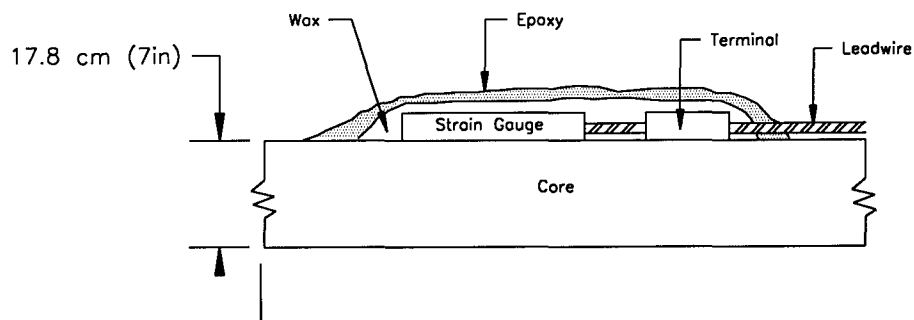
Figure 2b. Cross Section of Instrumented Core
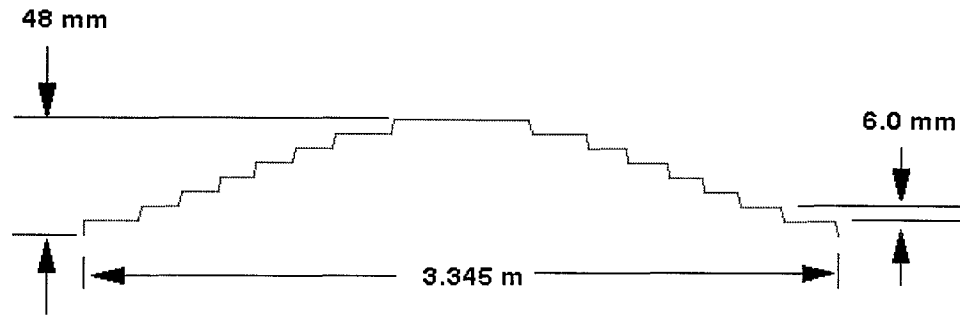
Figure 3a. Bump Dimensions
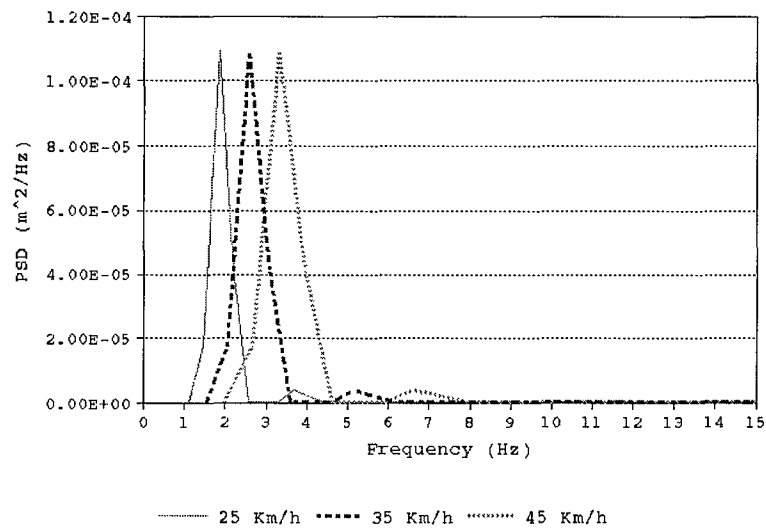
Figure 3b. Power Spectral Density of Bump

28
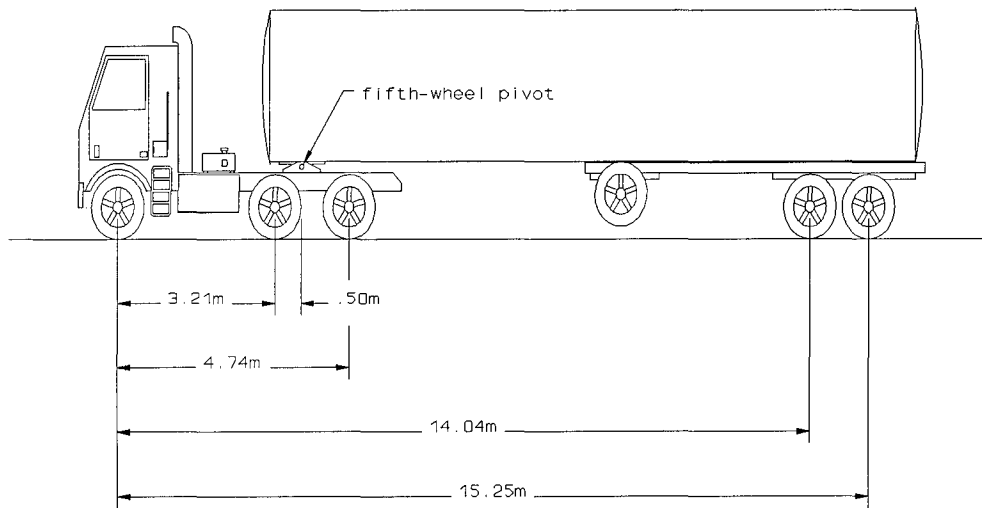
Figure 4a. NRC Truck Wheel Spacing
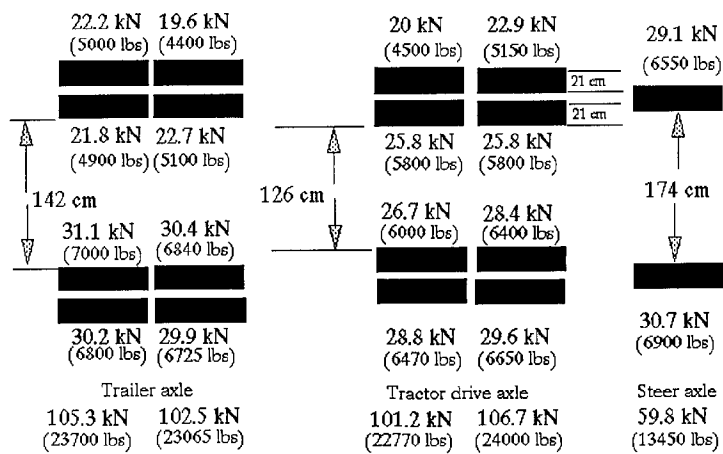
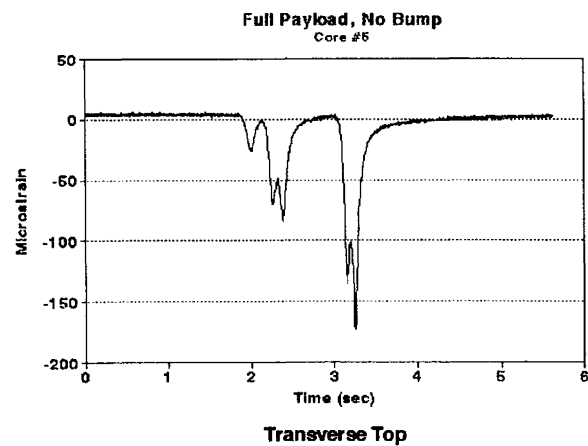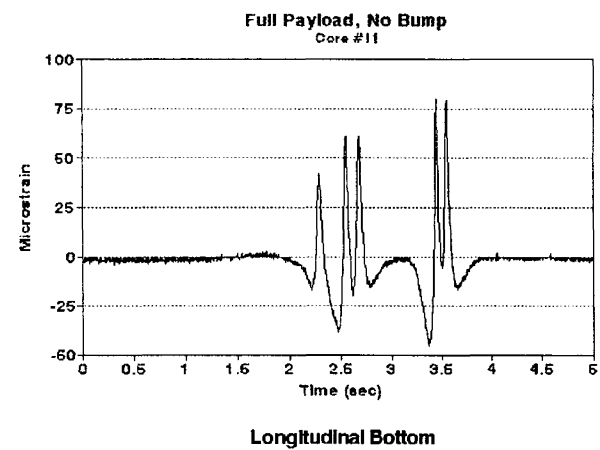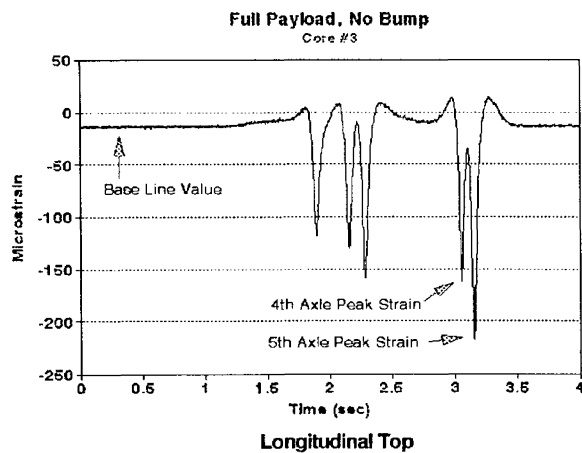**Figure 4b. NRC Truck Tire & Axle Weights, Full Load**
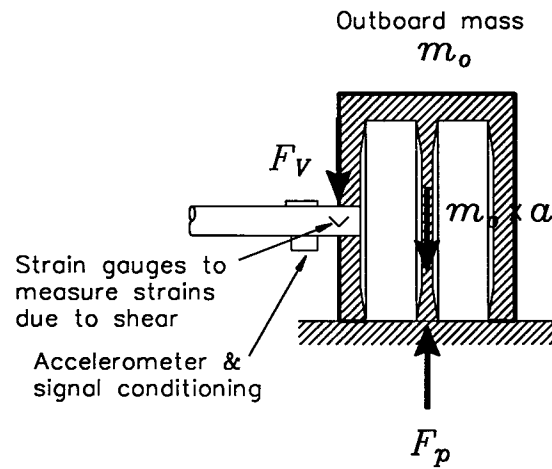
$$F_p = F_V + m_o \times a$$

where:

F_p Dynamic wheel force applied to the pavement

F_V Dynamic shear force measured in axle stub

m_o The mass outboard of the strain gauges

a The acceleration of the outboard mass (m).

Outboard mass m_o

F_V

$m_o \times a$

Strain gauges to measure strains due to shear

Accelerometer & signal conditioning

F_p

Figure 5. Dynamic Wheel Force Measurement

Full Payload, No Bump
Core #3

Longitudinal Top

Full Payload, No Bump
Core #11

Longitudinal Bottom

Full Payload, No Bump
Core #5

Transverse Top

Full Payload, No Bump
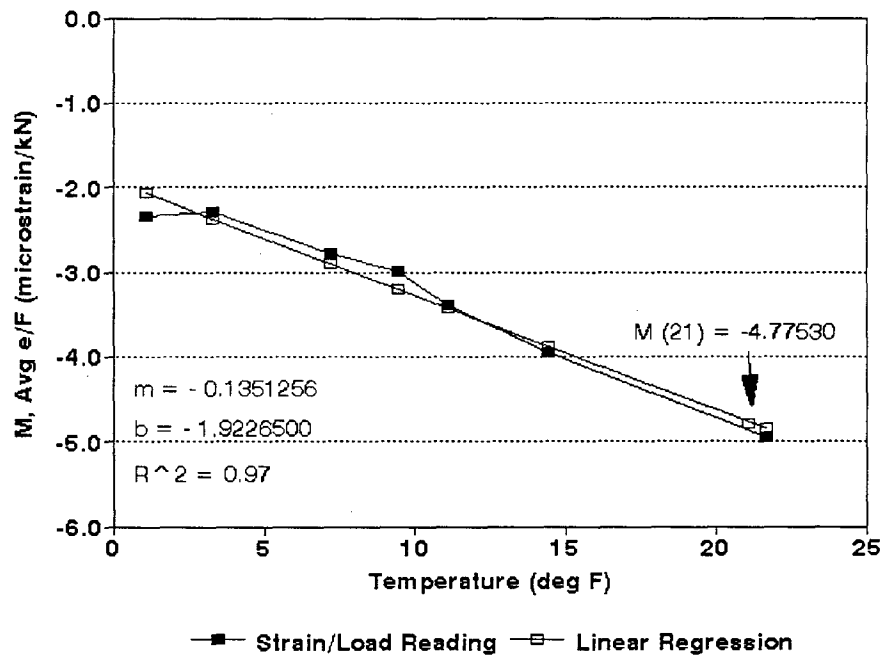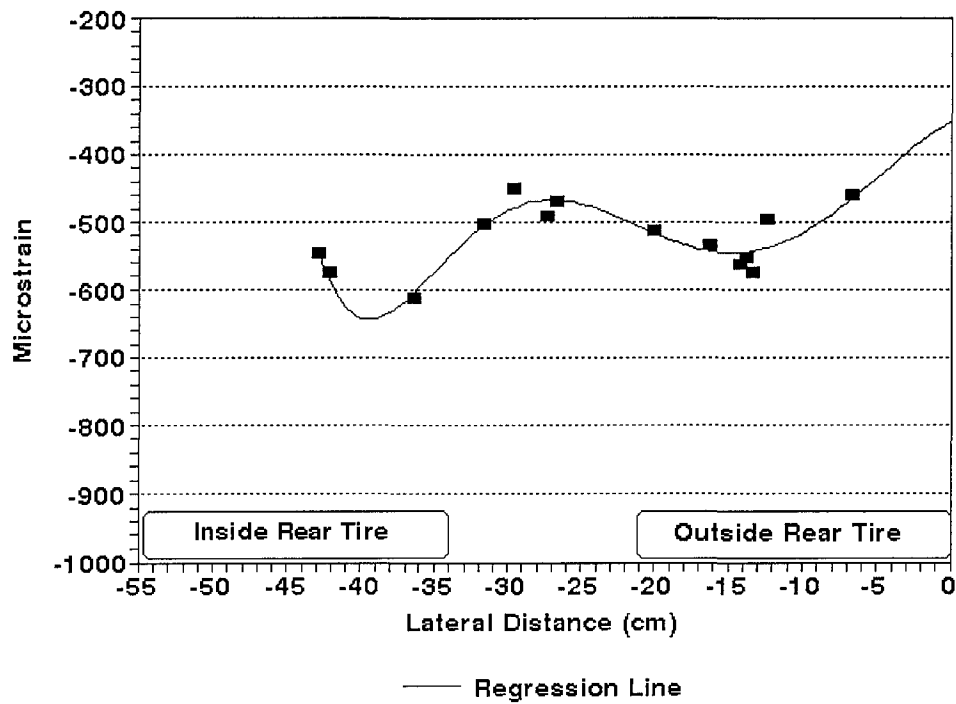Core #8

Transverse Bottom
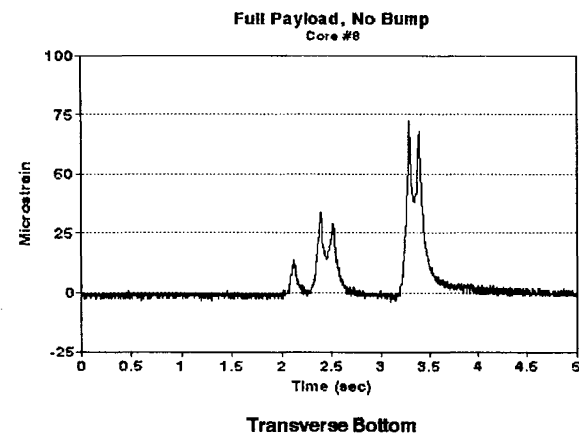
Figure 6. Uncalibrated Pavement Strain Traces, NRC Truck, 45 km/h
(Negatve is Compression, Positive is Tension)
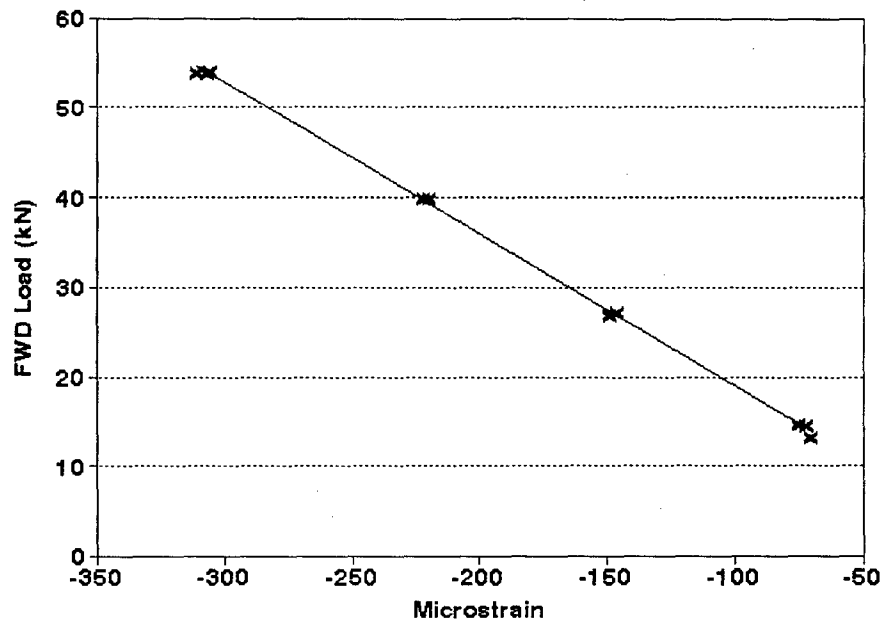
**Figure 7a. Load-Strain Relationship by FWD
LTOP (Core #0), T2 = 21.7 C**

**Figure 7b. Temperature Calibration
LTOP (All gauges) by FWD**

Regression Line Equation: $Y = A(x^6) + B(x^5) + C(x^4) + D(x^3) + E(x^2) + F(x) + G$

where;

$A = 3.06307 \times 10^{-6}$
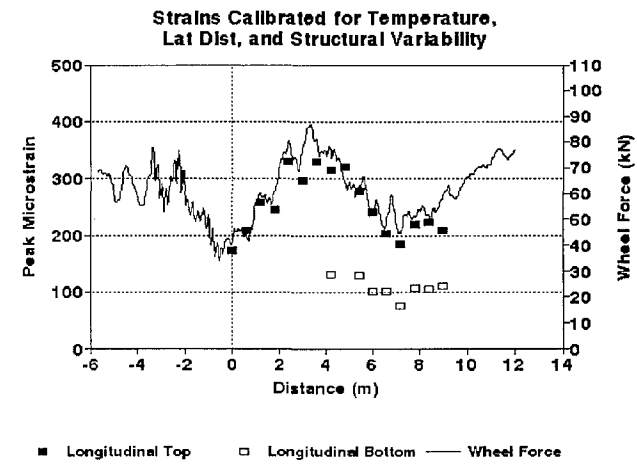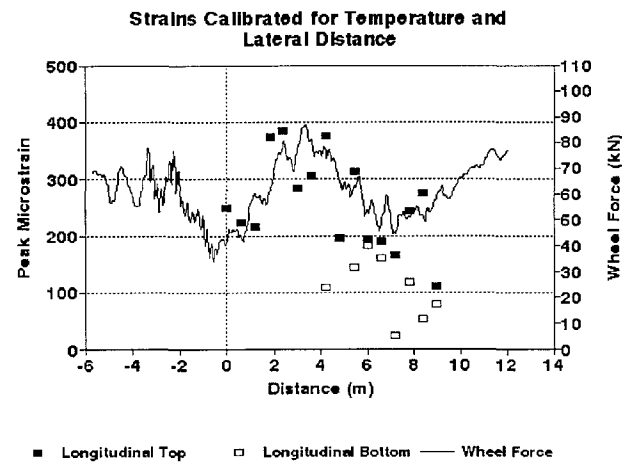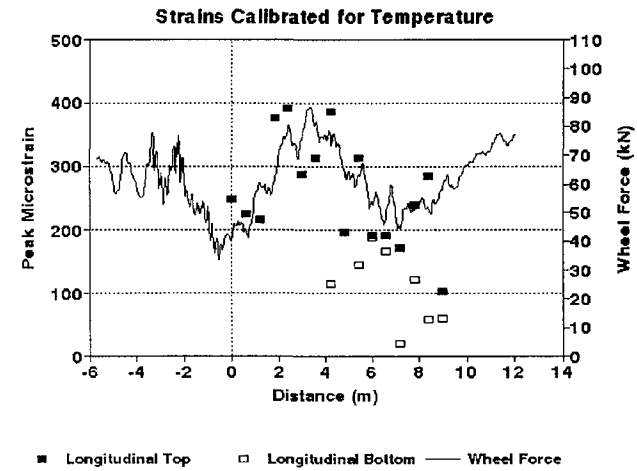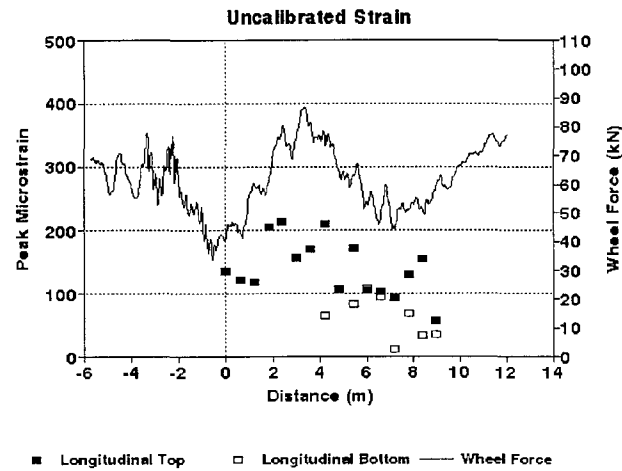$B = \ \ \ 0.000249459$
$C = \ \ \ 0.00461417$
$D = \ \ \ -0.0497649$
$E = \ \ \ -1.11323$
$F = \ \ \ 12.6813$
$G = \ \ \ -351.767$

**Figure 8. Lateral Distance Calibration
LTOP (Core #7)**

33

Uncalibrated Strain

Strains Calibrated for Temperature

Strains Calibrated for Temperature and Lateral Distance

Strains Calibrated for Temperature, Lat Dist, and Structural Variability

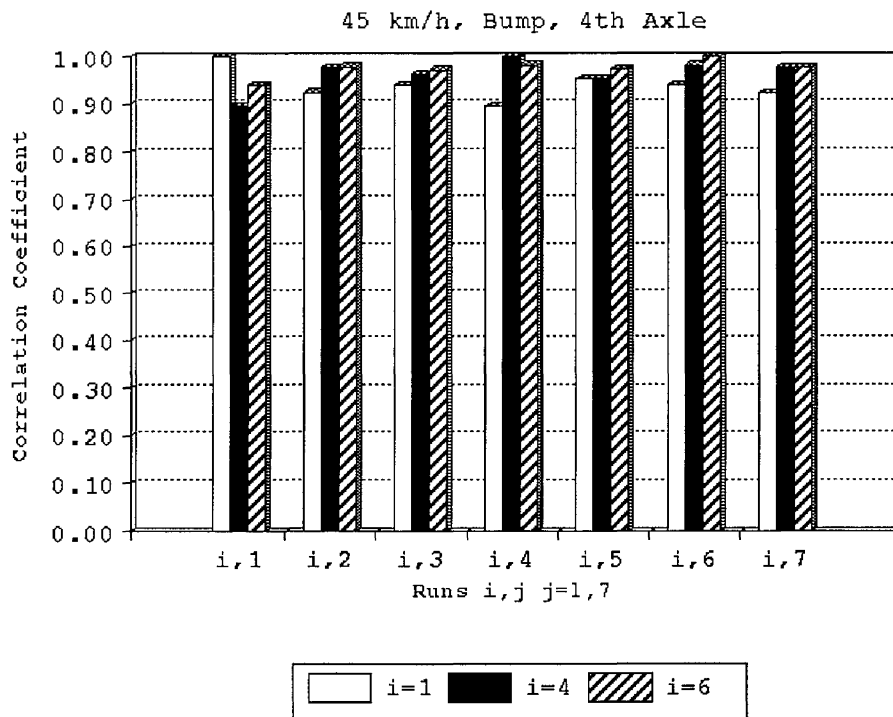■ Longitudinal Top   □ Longitudinal Bottom —— Wheel Force

Figure 9. The Three Stages of Gauge Calibration - 5th Axle
(All Peak Strain Values are plotted as positive to enable comparisons)
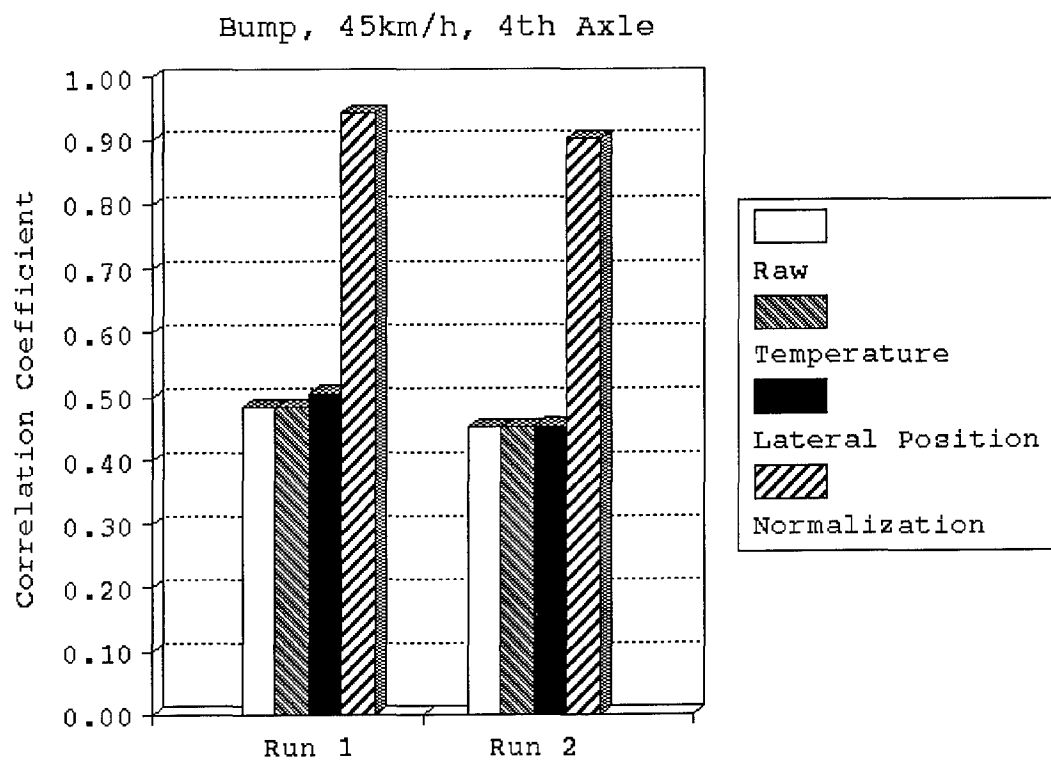
Figure 10. Effect of Calibrations on Load-Top Strain Correlations
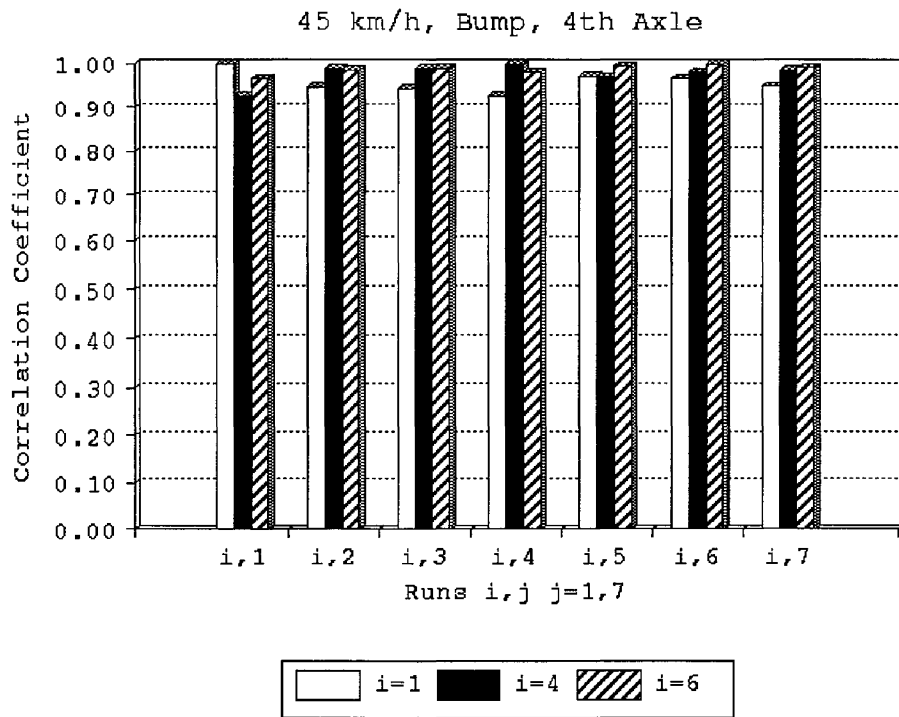
Figure 11a. Correlation Coefficients between Wheel Forces on Repeat Runs

Figure 11b. Correlation Coefficients between Top Strains on Repeat Runs
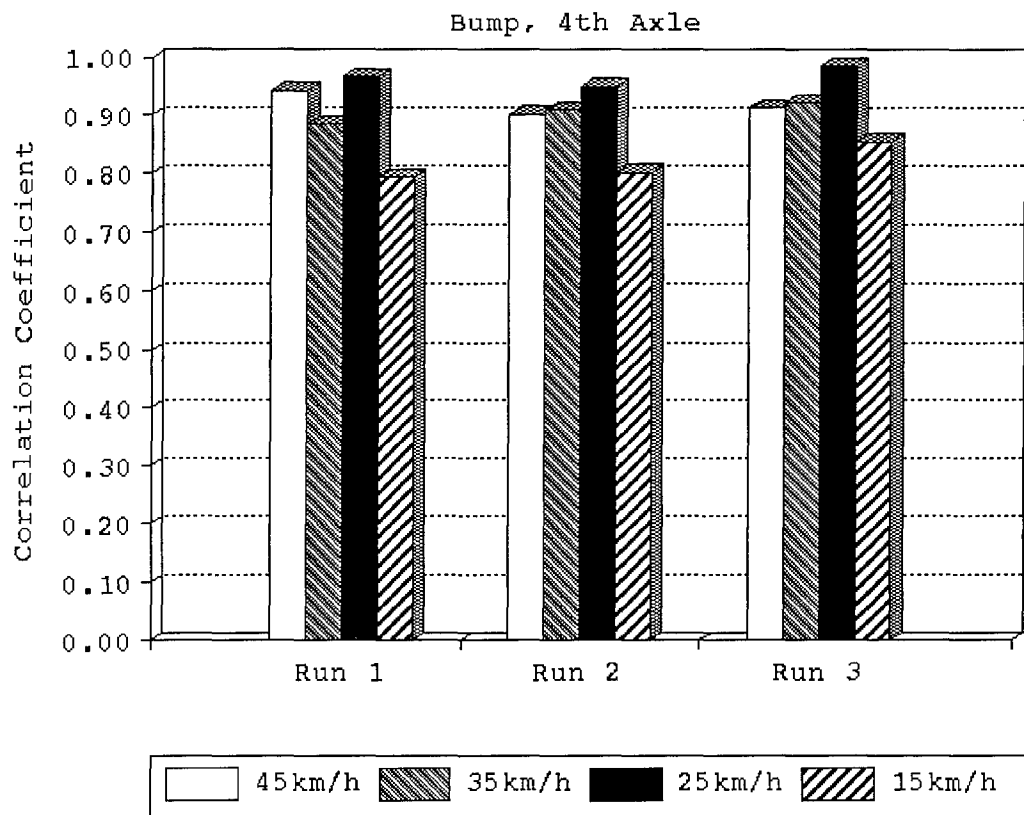
**Figure 12. Correlation Coefficients between
Wheel Forces & Top Peak Strain**

PSD of Wheel Forces
45 km/h, Run #1

PSD of Wheel Forces
35 km/h, Run #1

PSD of Wheel Forces
25 km/h, Run #1

PSD of Wheel Forces
15 km/h, Run #1
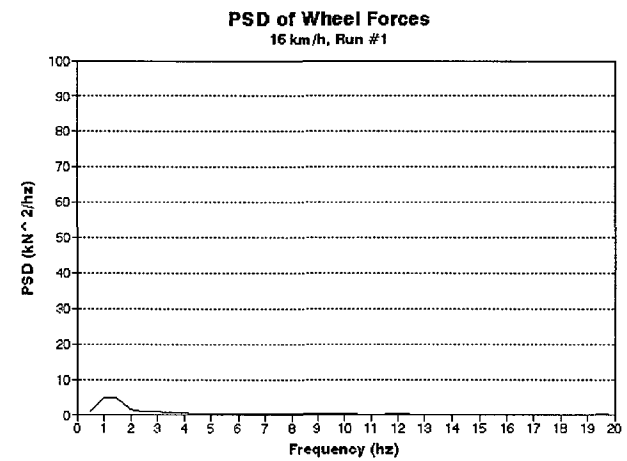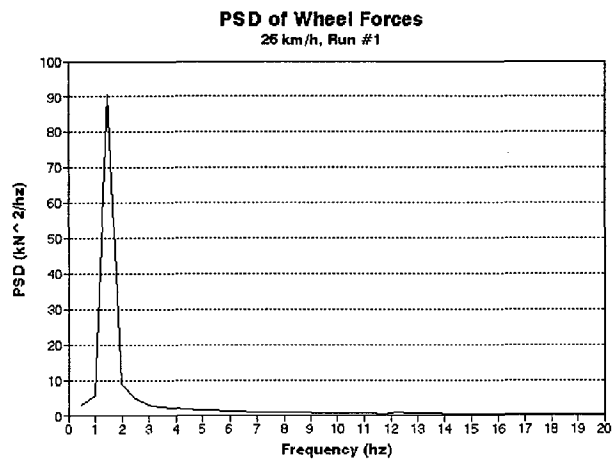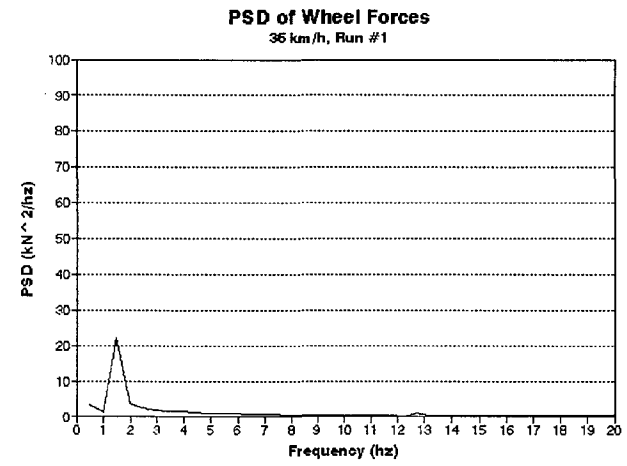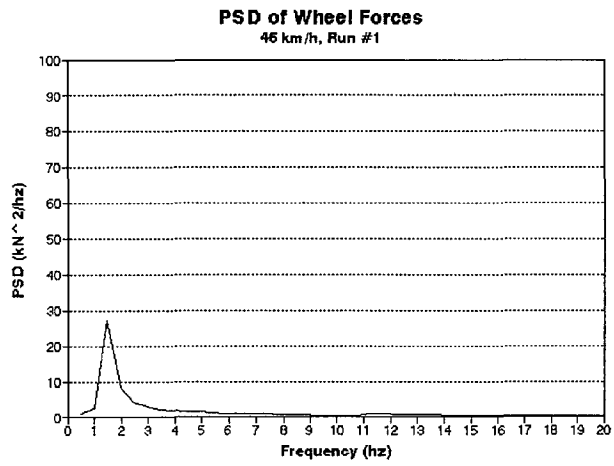
Figure 13a. Power Spectral Density (4th Axle, Bump)

PSD of Wheel Forces
45 km/h, Run #1

PSD of Wheel Forces
36 km/h, Run #2

PSD of Wheel Forces
26 km/h, Run #1

PSD of Wheel Forces
16 km/h, Run #1
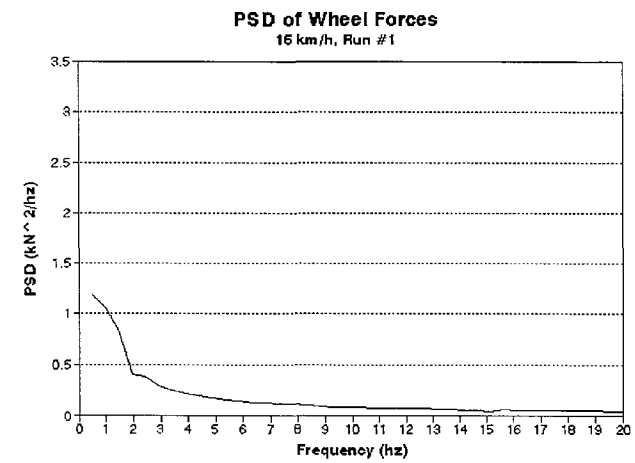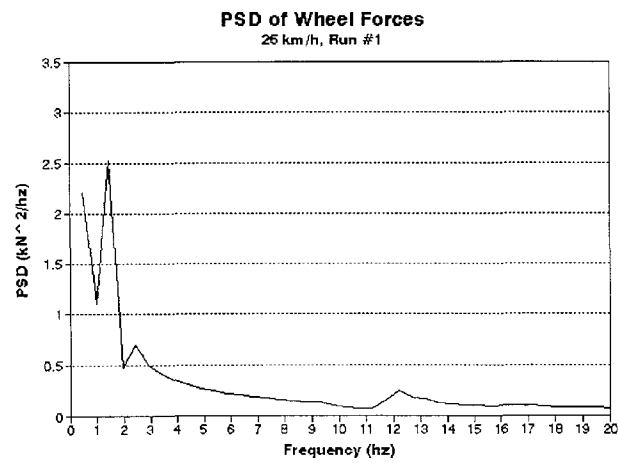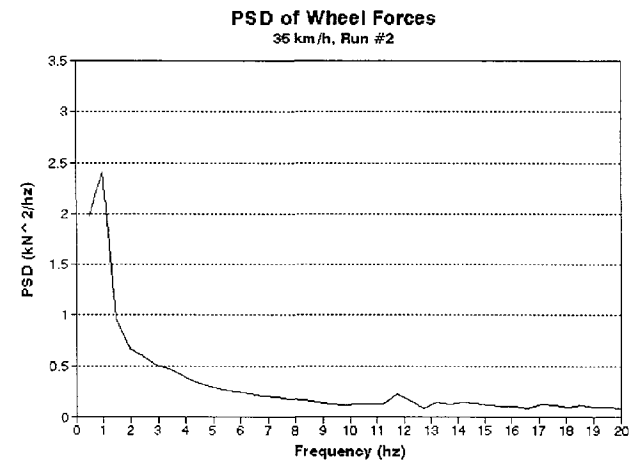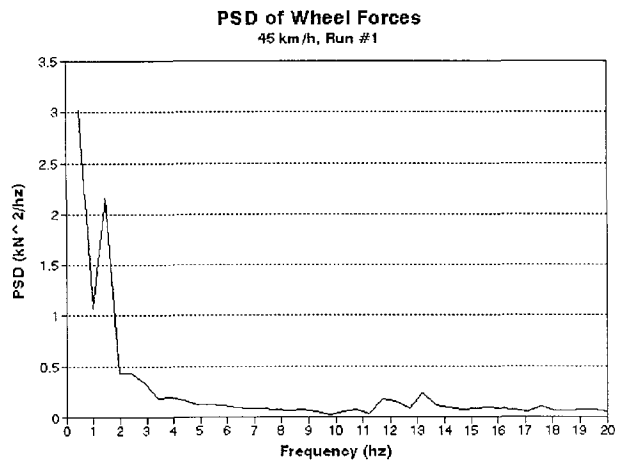
Figure 13b. Power Spectral Density (4th Axle, No Bump)
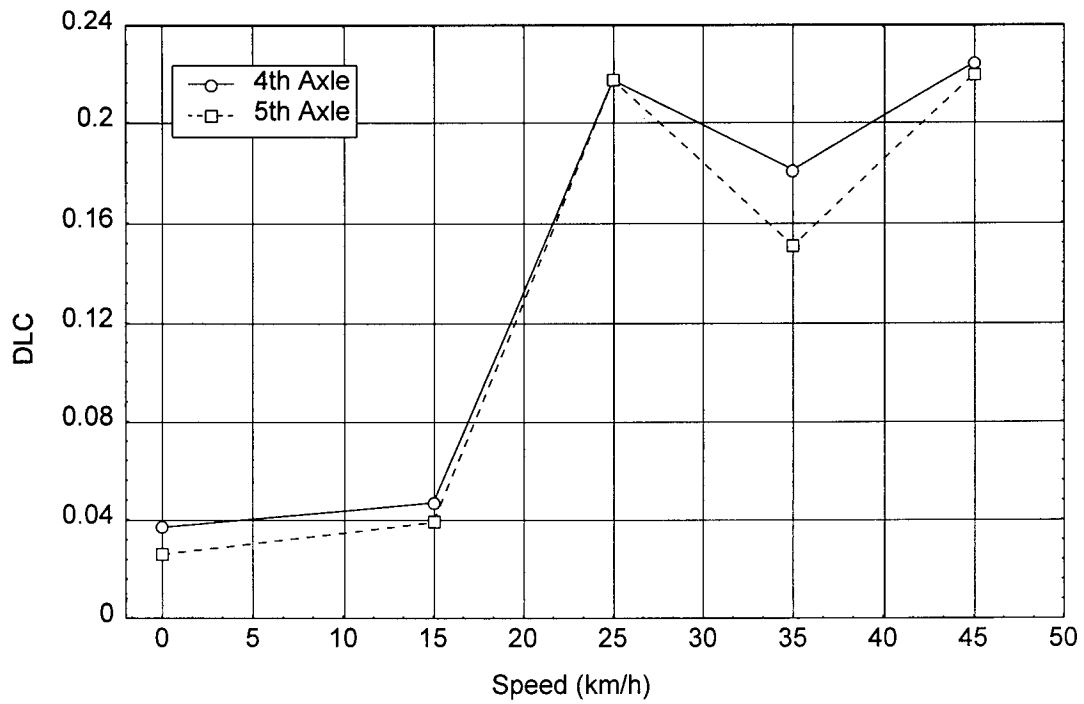
Figure 14a. DLC vs. Speed, with Bump
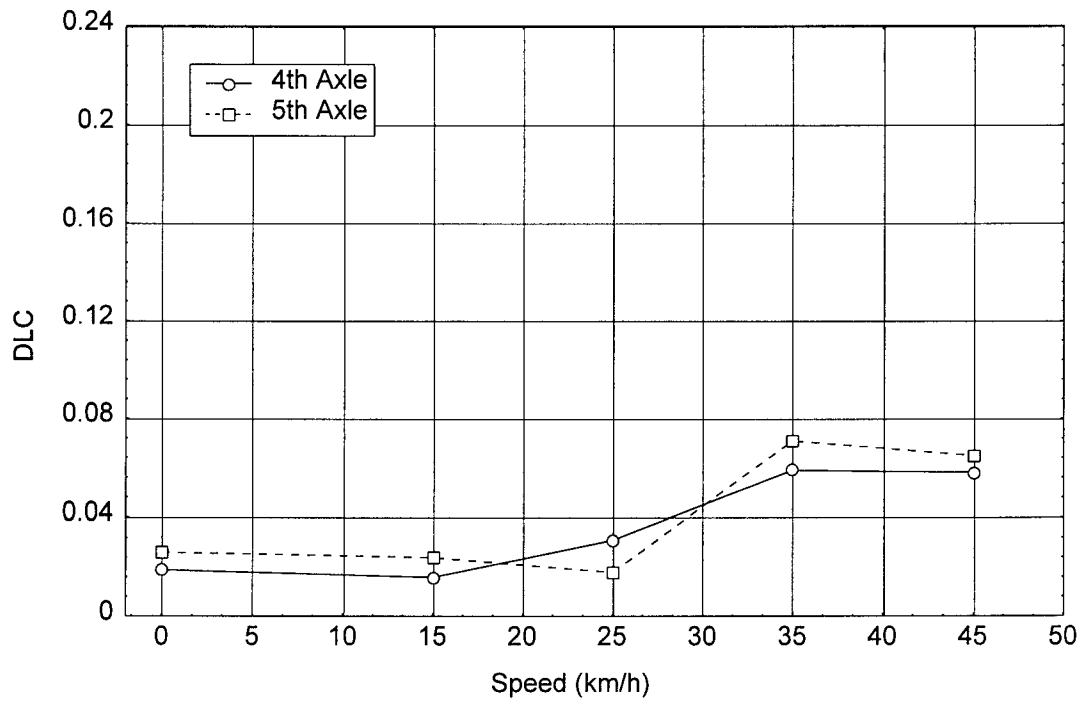
Figure 14b. DLC vs. Speed, No Bump
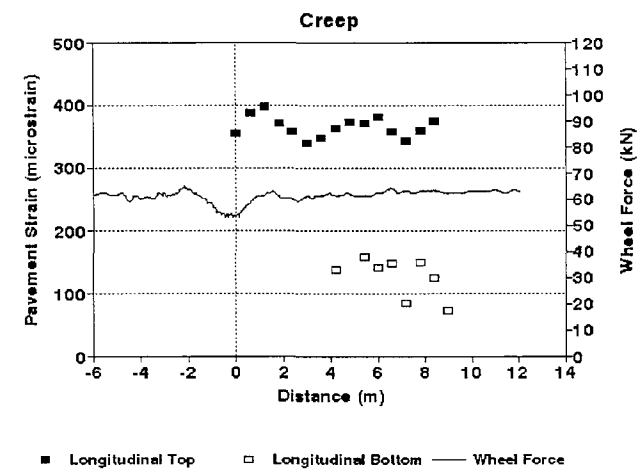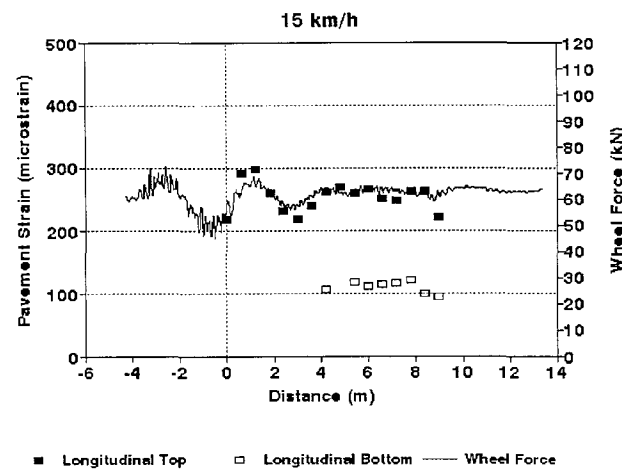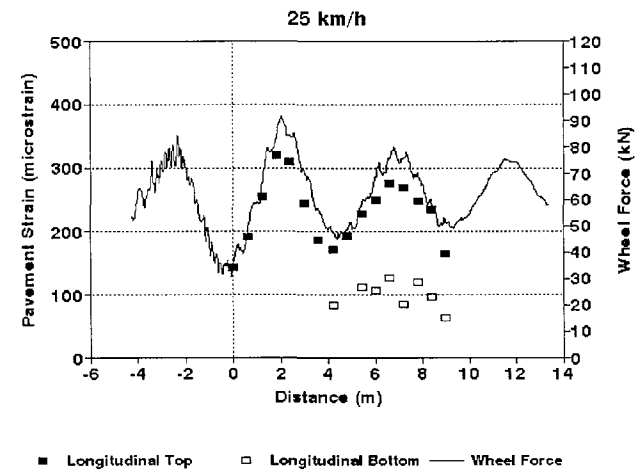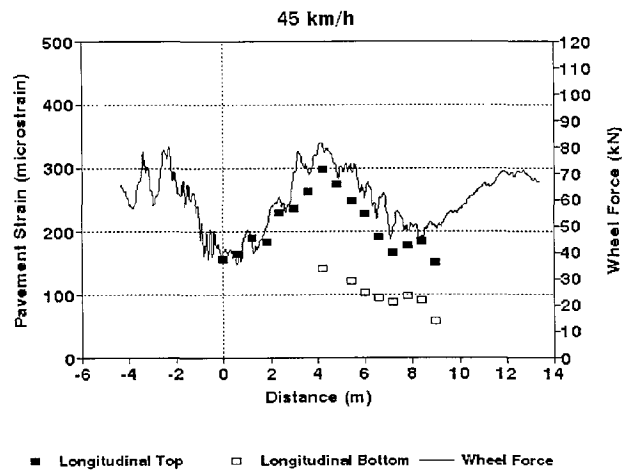
**Figure 15a. Peak Pavement Strain and Wheel Force Traces, With Bump, 4th Axle
(All Peak Strain Values are plotted as positive to enable comparisons)**
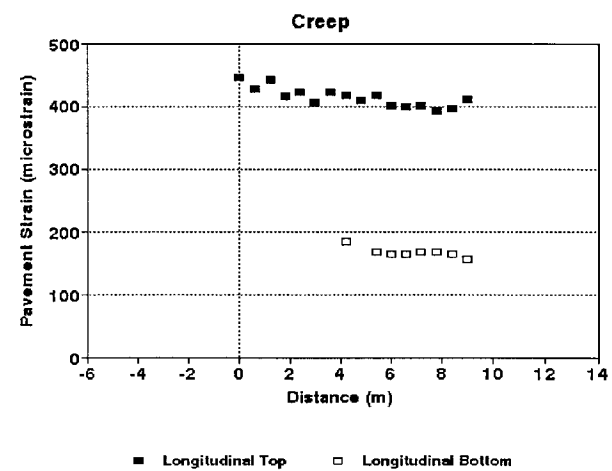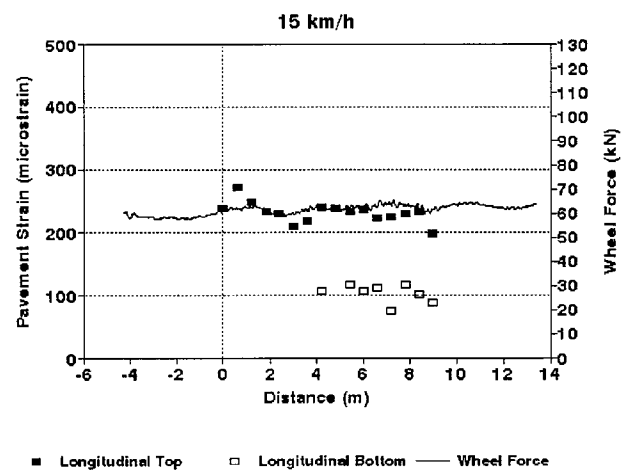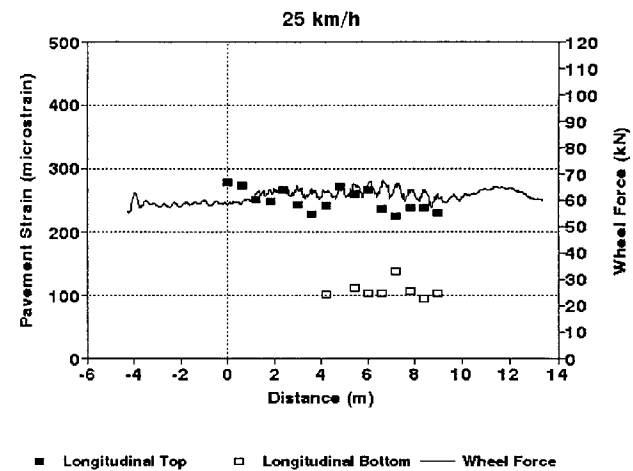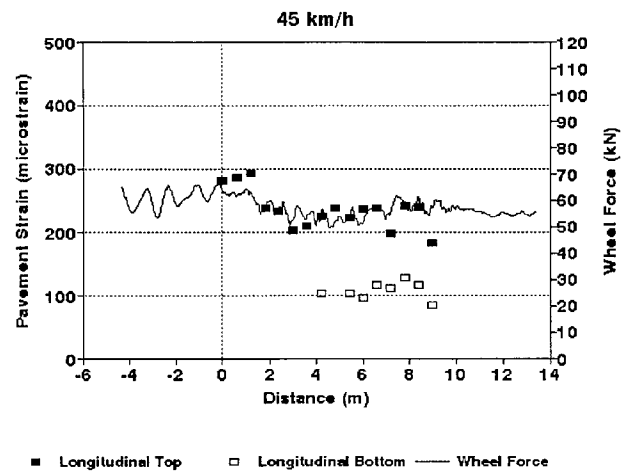
**Figure 15b. Peak Pavement Strain and Wheel Force Traces, No Bump, 4th Axle
(All Peak Strain Values are plotted as positive to enable comparisons)**
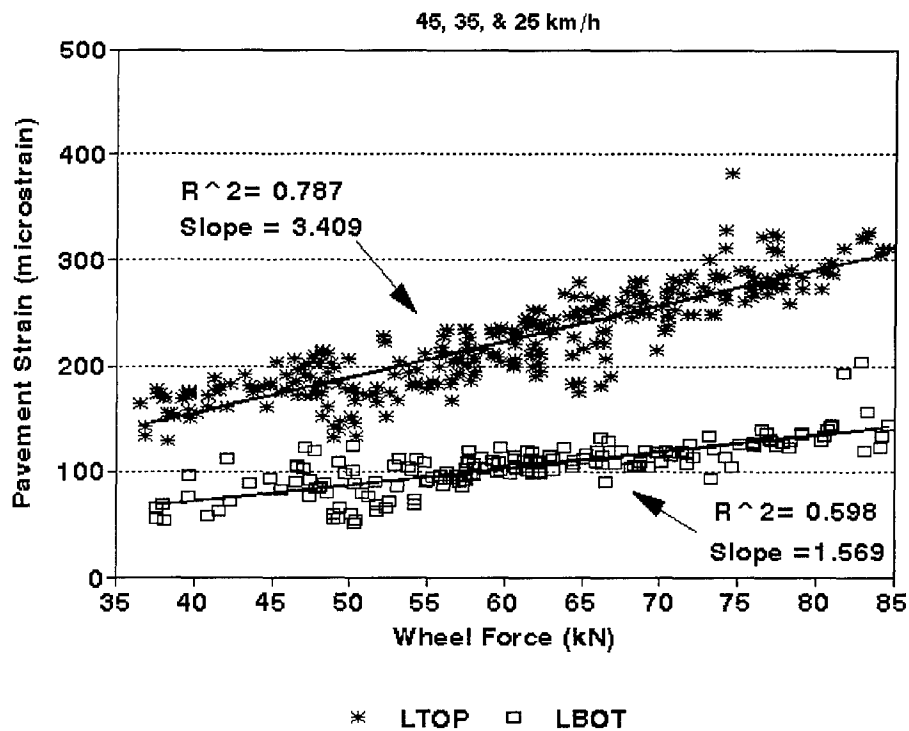
Figure 16a. Pavement Strain vs. Wheel Force, 4th Axle, With Bump
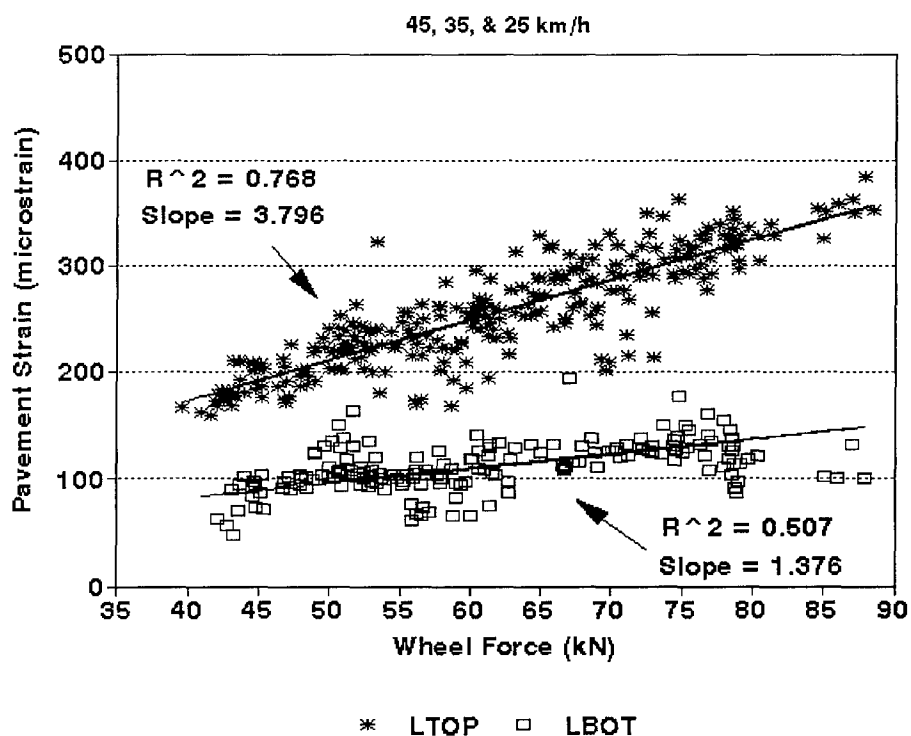
Figure 16b. Pavement Strain vs. Wheel Force, 5th Axle, With Bump
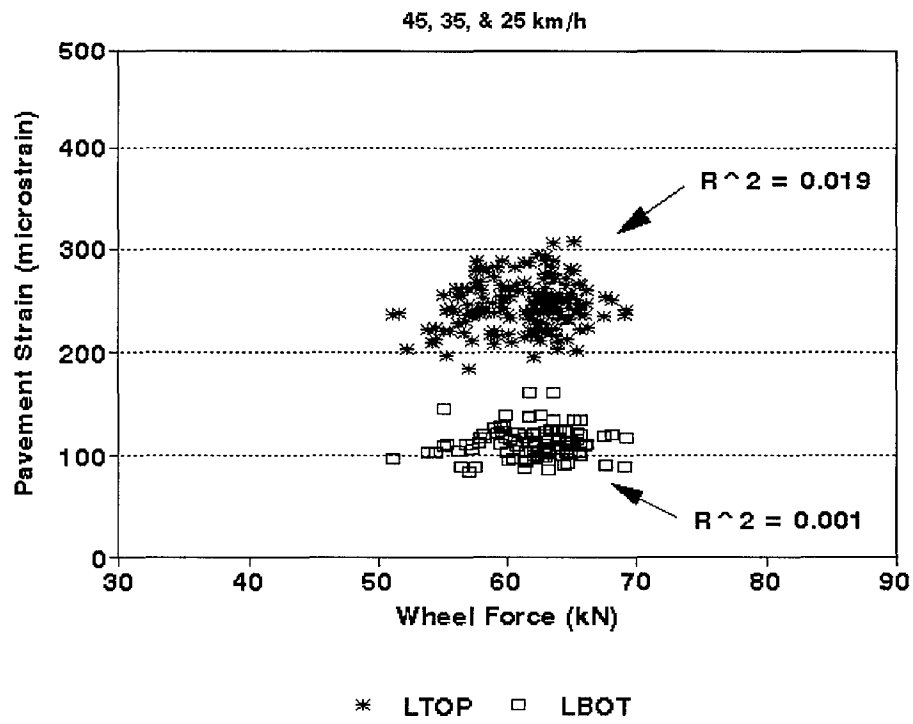
Figure 16c. Pavement Strain vs. Wheel Force, 4th Axle, No Bump
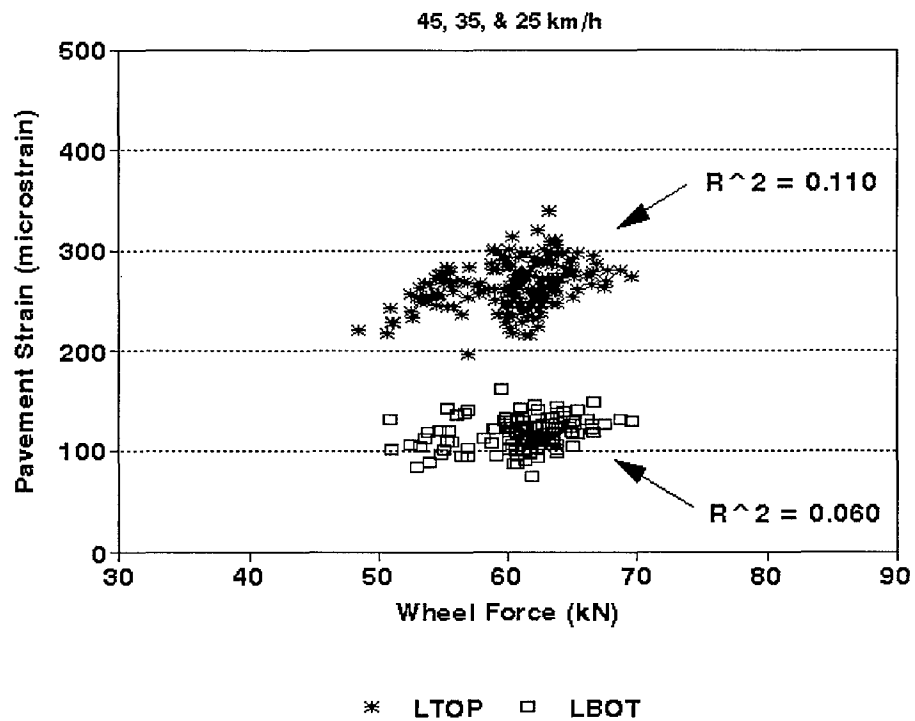
Figure 16d. Pavement Strain vs. Wheel Force, 5th Axle, No Bump

44
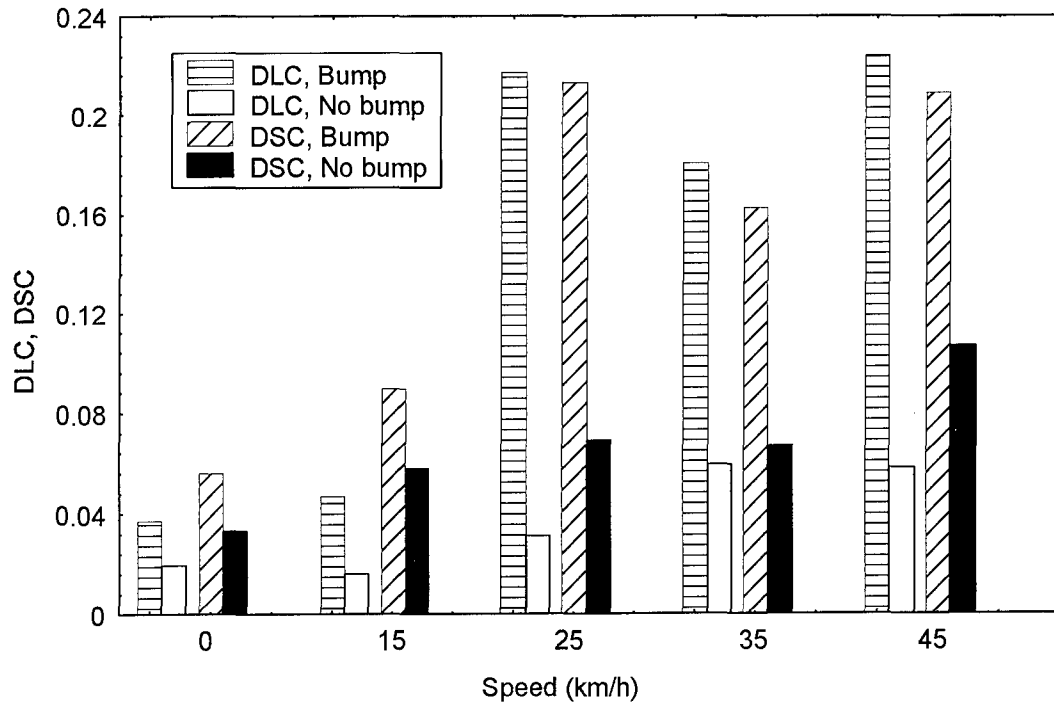
Figure 17a. DLC of 4th Axle and DSC of Top Gauges (Average Values)
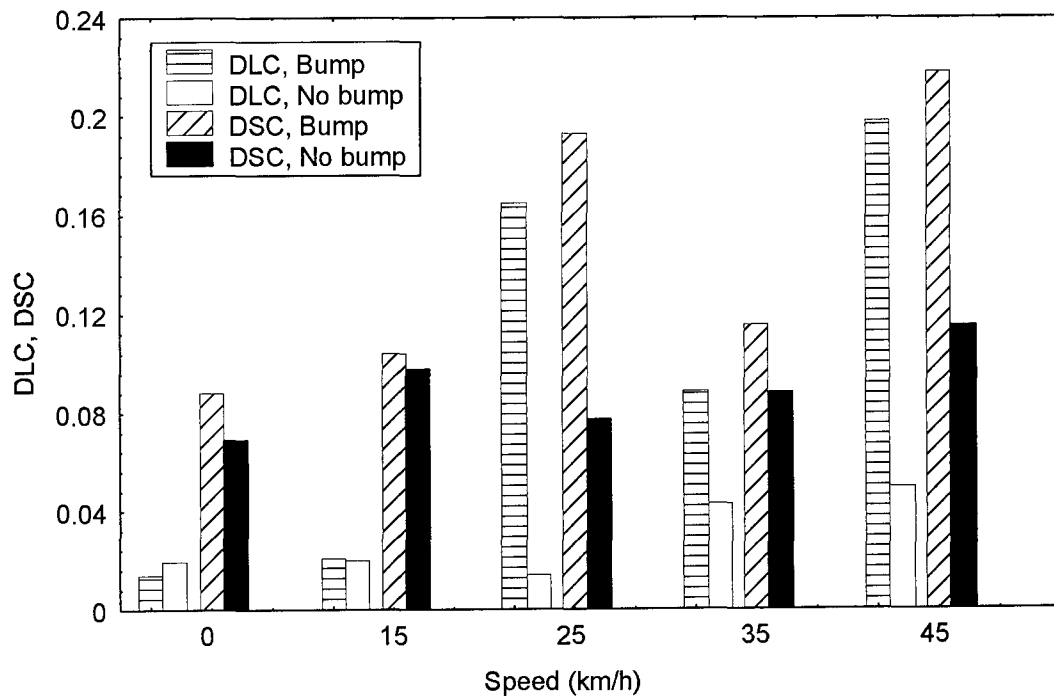
Figure 17b. DLC of 4th Axle and DSC of Bottom Gauges (Average Values)
(DLC and DSC for Bottom Gauges Calculated Using 8 of 16 Points)
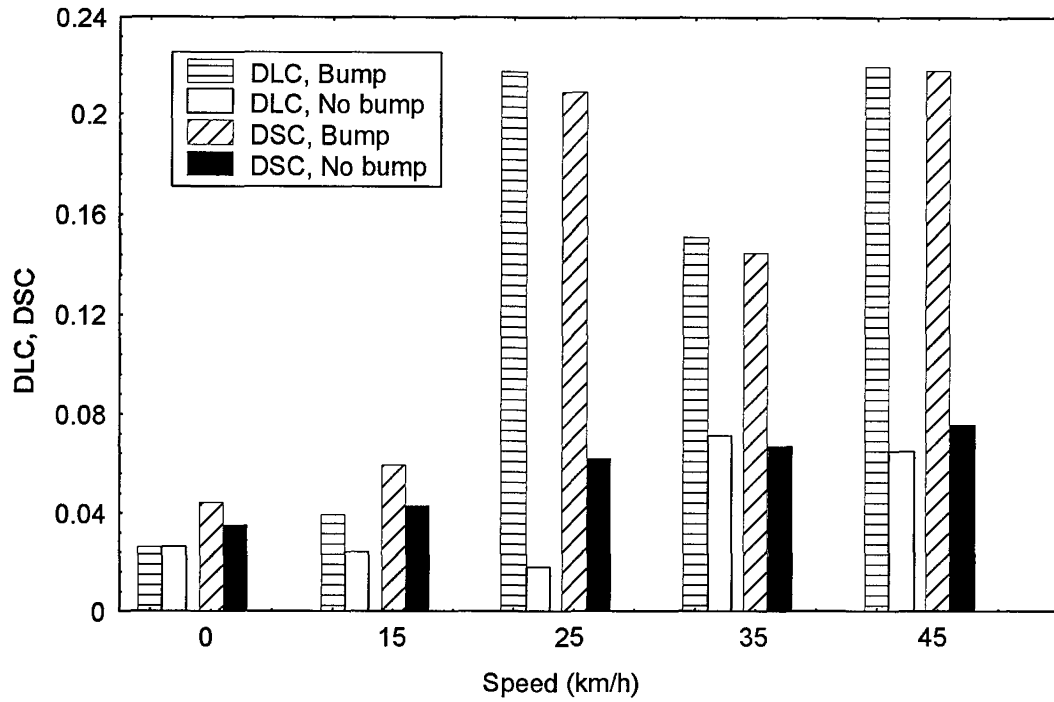
Figure 17c. DLC of 5th Axle and DSC of Top Gauges (Average Values)
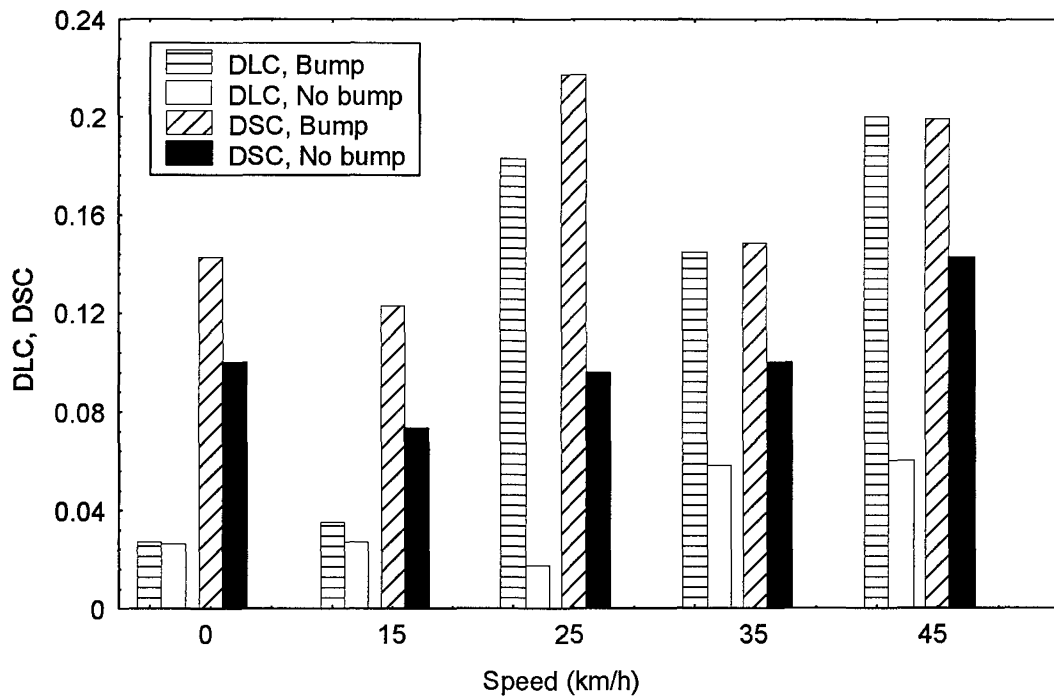
Figure 17d. DLC of 5th Axle and DSC of Bottom Gauges (Average Values)
(DLC and DSC for Bottom Gauges Calculated Using 8 of 16 Points)
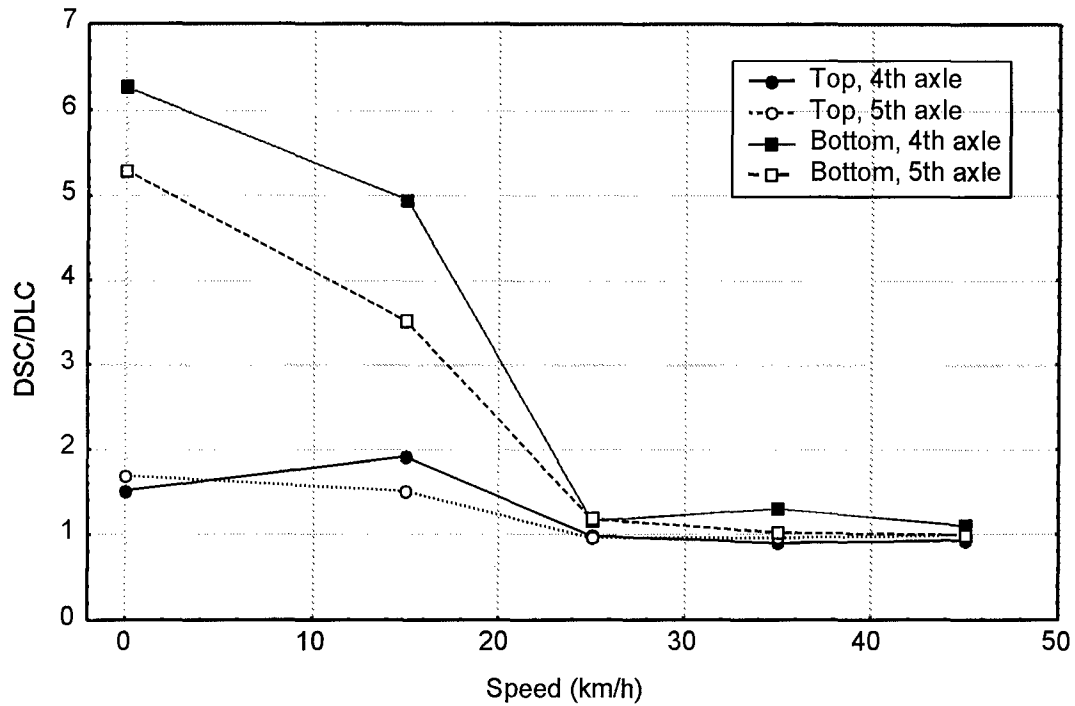
Figure 18a. Ratio of DSC and DLC vs. Speed, with Bump
(DLC and DSC for Bottom Gauges Calculated Using 8 of 16 Points)
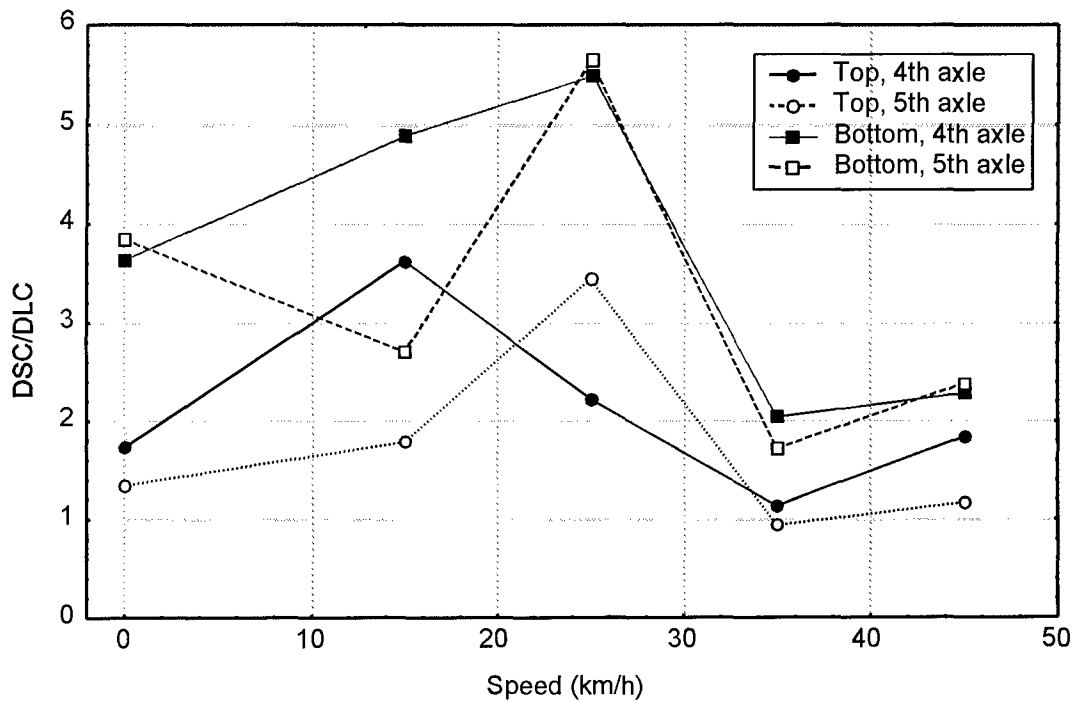
Figure 18b. Ratio of DSC and DLC vs. Speed, No Bump
(DLC and DSC for Bottom Gauges Calculated Using 8 of 16 Points)
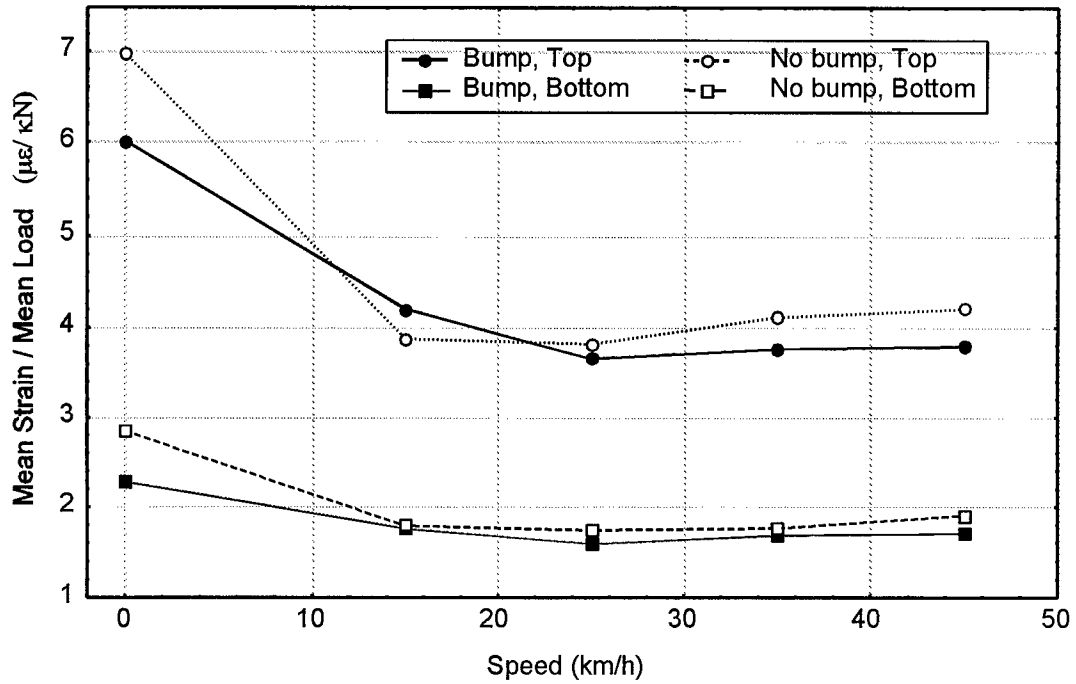
Figure 19a. Viscoelastic Effect, 4th Axle (Average of Runs)
(Mean Values for Bottom Gauges Calculated Using 8 of 16 Points)
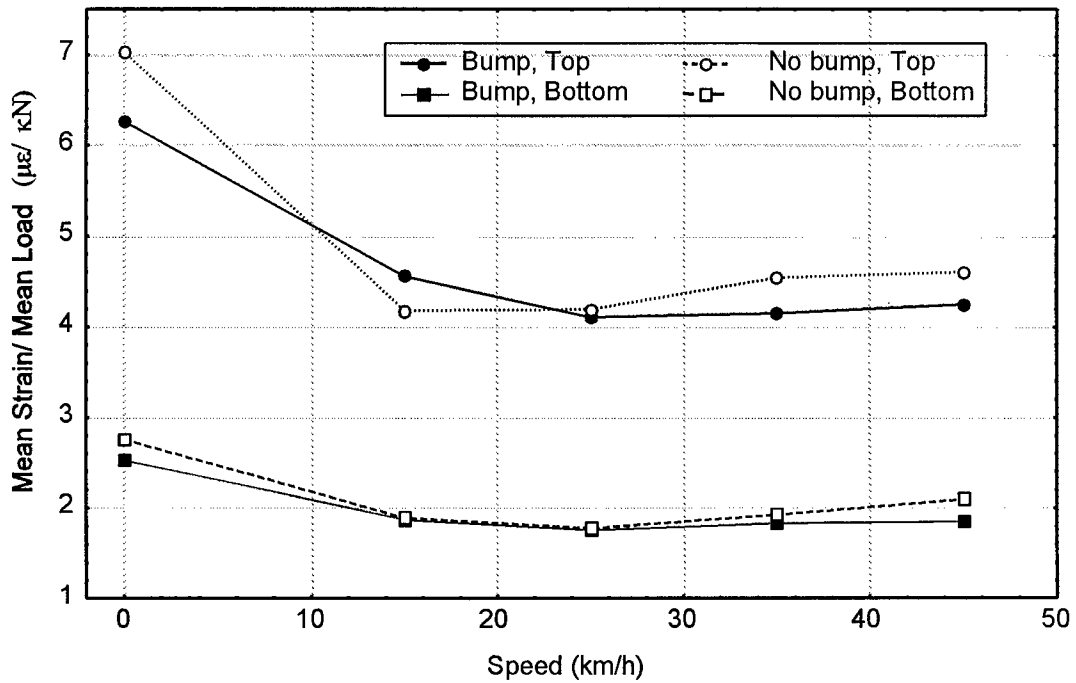
Figure 19b. Viscoelastic Effect, 5th Axle (Average of Runs)
(Mean Values for Bottom Gauges Calculated Using 8 of 16 Points)
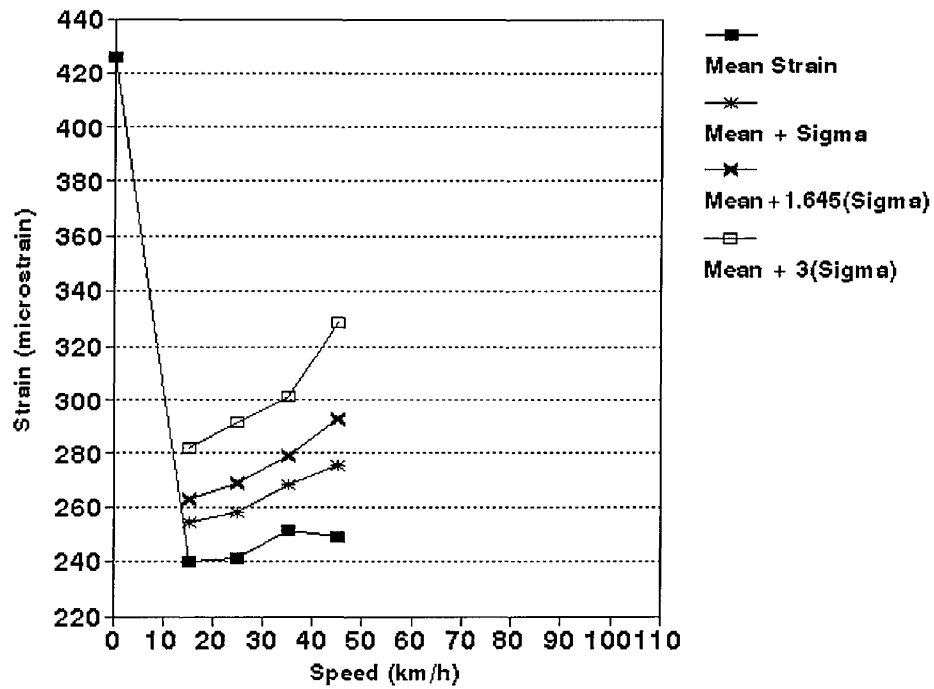
Figure 20a. Speed Effect, Longitudinal Top Gauges, 4th Axle, No Bump
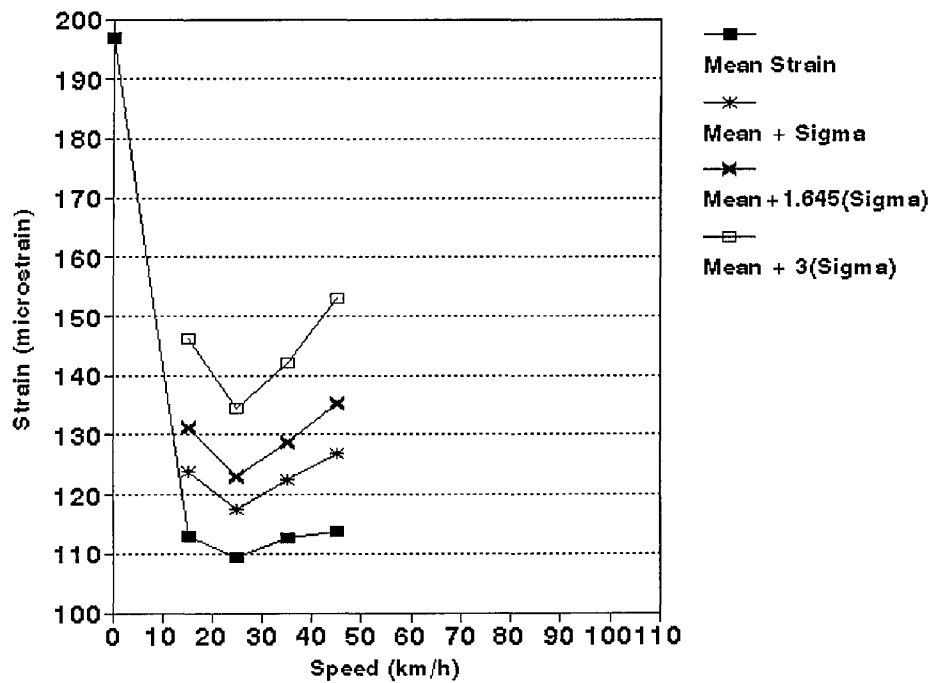
Figure 20b. Speed Effect, Longitudinal Bottom Gauges, 4th Axle, No Bump
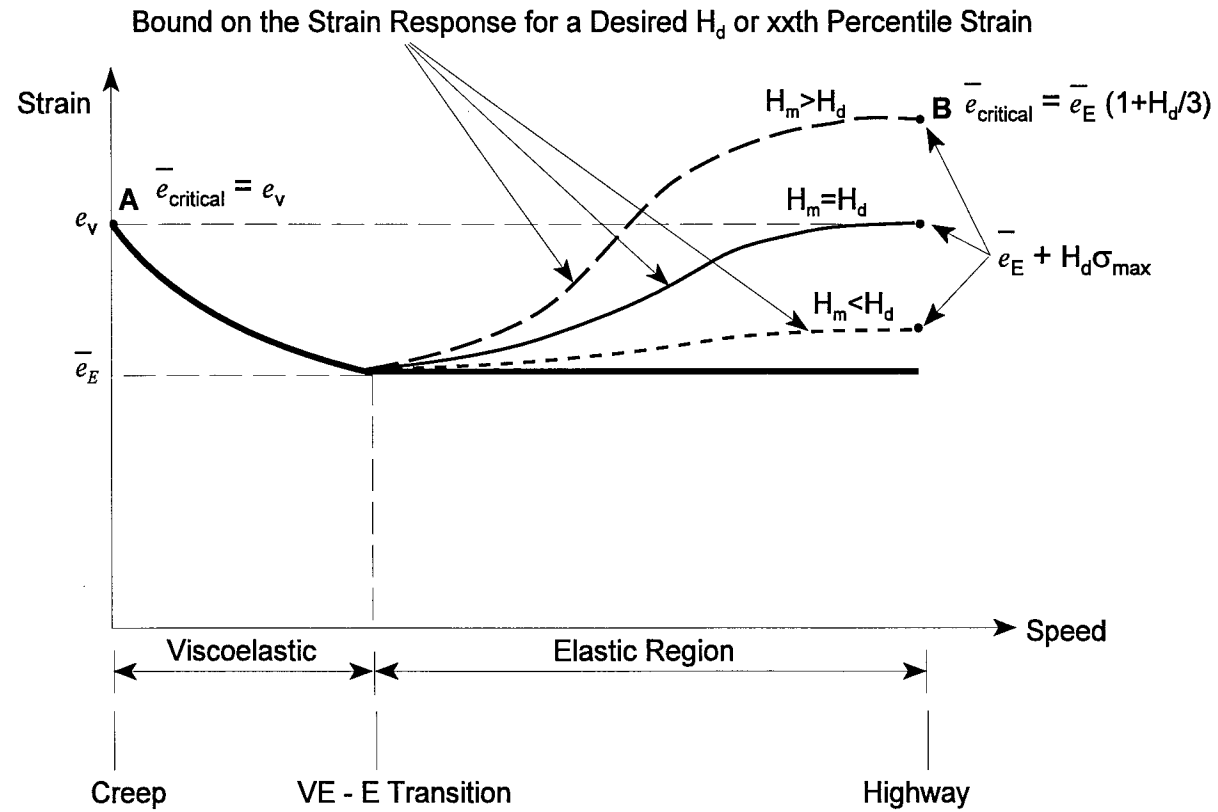
Figure 21. Critical Strain Response to Dynamic Moving Load. After [7]

	FHWA PROGRAM	FHWA/DIVINE PROGRAM	FINLAND PROGRAM
PAVEMENT THICKNESS (mm)	152	Same	B - 150
			C - 80
TRUCKS	FHWA (2-Axle)	NRC (5-Axle)	VIRTTAA (2-Axle)
	NRC (5-Axle) (Lift Axle Up/Down)		TRL (2-Axle)
			NRC (5-Axle) (Lift Axle Up)
SUSPENSION	FHWA - Air & Steel	NRC - Air	VIRTTAA - Steel
	NRC - Air		TRL - Steel
			NRC - Air
AXLES	FHWA, NRC All Axles Tested	Trailer Tandem Set	
GAUGES	Length = 50 mm	Longitudinal Top & Bottom Gages	Length = 70mm
	16 Longitudinal Top 16 Longitudinal Bottom 16 Transverse Top 16 Transverse Bottom		B Pavement 13 Top,12 Bottom
			C Pavement 19 Top,13 Bottom
BUMPS	No Bump	Same	No Bump
	3.3 m X 50 mm	Same	4 m X 50 mm
			0.3 m X 25 mm
SPEED (km/h)	FHWA - 0,25,40,55,70	0,15,25,35,45	TRL - 45
	NRC - 0,15,25,35,45		NRC - 45
			VIRTTAA- 45
PRESSURE (kPa)	FHWA - STEEL 620	760	VIRTTAA - 760
	FHWA - AIR 620, 760, 860		TRL - 760
	NRC - 760		NRC - 760
PAYLOAD	FHWA - AIR 14k, 6k, & 0 lbf	Full Load	
	FHWA - STEEL 14k, 6k, & 0 lbf		
	NRC - Full/No Load		NRC-Full Load

TABLE 1. FHWA, Finland, & FHWA/DIVINE Testing Programs Summary

PAVEMENT TEMPERATURE	FWD LOAD (F)		PEAK STRAIN (e)	STRAIN / LOAD (e/F)
	kN	(lb)	(microstrain)	(microstrain/kN)
			CORE #0 L-top	
	13.22	(2971)	-70	-5.295
T1 = 23.3 C (74 F)	14.69	(3300)	-75	-5.107
T2 = 21.7 C (71 F)	14.62	(3286)	-72	-4.924
T3 = 18.9 C (66 F)	26.90	(6045)	-149	-5.539
	27.29	(6133)	-146	-5.350
	27.22	(6117)	-146	-5.364
	39.97	(8982)	-220	-5.504
	39.98	(8984)	-222	-5.553
	39.91	(8969)	-220	-5.512
	53.85	(12102)	-307	-5.701
	53.81	(12092)	-311	-5.780
	54.08	(12153)	-306	-5.658
				-5.440 =Avg (e/F) Core 0

TABLE 2.   Test Results Conducted on October 19, 1994

52

Avg. e/F Values from 12/2/94		Avg. e/F Values from 2/2/95		Avg. e/F Values from 2/21/95		Avg. e/F Values from 2/23/95	
Pavement Temperature;		Pavement Temperature;		Pavement Temperature;		Pavement Temperature;	
Average T2 = 1.1 C (34 F)		Average T2 = 3.3 C (38 F)		Average T2 = 7.2 C (45 F)		Average T2 = 9.4 C (49 F)	
	L-top		L-top		L-top		L-top
	Avg. e/F		Avg. e/F		Avg. e/F		Avg. e/F
CORE#	(microstrain/kN)	CORE#	(microstrain/kN)	CORE#	(microstrain/kN)	CORE#	(microstrain/kN)
0	-2.722	0	*	0	*	0	*
1	-2.447	1	-2.530	1	-3.355	1	-3.247
2	-2.082	2	-2.545	2	-3.091	2	-3.064
3	-3.363	3	-3.859	3	-5.036	3	-5.274
4	-2.882	4	-2.173	4	-2.256	4	-2.921
5	-1.971	5	-2.352	5	-2.819	5	-2.746
6	-1.981	6	-2.339	6	-2.789	6	-2.917
7	-2.702	7	-3.038	7	-3.442	7	-4.039
8	-1.769	8	-1.795	8	-2.114	8	-2.295
9	-2.688	9	-2.979	9	-3.565	9	-3.660
10	-1.919	10	-2.002	10	-1.653	10	-1.948
11	-2.277	11	-2.294	11	-3.177	11	-3.147
12	-2.201	12	*	12	*	12	*
13	-2.268	13	-1.384	13	-2.434	13	-2.538
14	-3.206	14	-2.370	14	-2.602	14	-3.442
15	-1.182	15	-0.562	15	-0.599	15	-0.637
AVG. All Cores (M) =	-2.337	AVG. All Cores (M) =	-2.292	AVG. All Cores (M) =	-2.787	AVG. All Cores (M) =	-2.991

Avg. e/F Values from 11/29/94		Avg. e/F Values from 3/8/95		Avg. e/F Values from 10/19/94	
Pavement Temperature;		Pavement Temperature;		Pavement Temperature;	
Average T2 = 11.1 C (52 F)		Average T2 = 14.4 C (58 F)		Avgerage T2 = 21.7 C (71 F)	
	L-top		L-top		L-top
	Avg. e/F		Avg. e/F		Avg. e/F
CORE#	(microstrain/kN)	CORE#	(microstrain/kN)	CORE#	(microstrain/kN)
0	-3.590	0	*	0	-5.440
1	-3.401	1	-4.202	1	-6.002
2	-2.655	2	-3.783	2	-3.836
3	-5.194	3	-6.878	3	-6.612
4	-4.551	4	-5.757	4	-5.656
5	-2.771	5	-3.401	5	-4.259
6	-2.800	6	-3.637	6	-4.434
7	-3.693	7	-2.839	7	-5.175
8	-2.265	8	-2.654	8	-3.281
9	-3.793	9	-4.755	9	-5.075
10	-2.842	10	-2.713	10	-3.852
11	-3.097	11	-4.287	11	-4.529
12	-2.995	12	*	12	-5.156
13	-3.505	13	-4.045	13	-4.923
14	-4.709	14	-5.580	14	-7.028
15	-2.161	15	-0.982	15	-4.302
AVG. All Cores (M) =	-3.389	AVG. All Cores (M) =	-3.955	AVG. All Cores (M) =	-4.942

* Bad Strain Reading, not included in any of the seven AVG (M) values.

TABLE 3.   Average Strain/Load Ratios
(Longitudinal Top Gauges)

FWD Testing Dates:	Pavement Temperature (deg C) (T2)	Avg e/F All Cores (LTOP's) (microstrain/kN) M(T2)	Linear Fit Value (microstrain/kN) M(T2)
Dec 2, '94	1.1	-2.337	-2.073
Feb 2, '95	3.3	-2.292	-2.373
Feb 21, '95	7.2	-2.787	-2.899
Feb 23, '95	9.4	-2.991	-3.199
Nov 29, '94	11.1	-3.389	-3.424
March 8, '95	14.4	-3.955	-3.874
Oct 19, "94	21.7	-4.942	-4.850
	21.1	M(21) =	-4.77530

* Linear Fit Values are the e/F values that fall on the linear-fit line at the respective pavement temperatures.

Table 4. Avg. Strain/Load Ratios Summary
(Longitudinal Top Gauges)

A	B	C	D	E	F
Run #	Pavement Temperature (^{0}C) T2	Lateral Distance (cm) X	Peak Strain (μe) $e_{T2,x}$	Temperature Calibration Factor CF$_{21}$	Temperature Corrected Peak Strain (μe) $e_{21,x}$
1	11.1	-29.6	-322.3	0.717	-449
2	12.2	-31.6	-376.9	0.748	-503
3	12.2	-13.8	-412.8	0.748	-551
4	12.8	-16.2	-406.8	0.764	-532
5	12.8	-14.2	-428.7	0.764	-561
6	12.8	0.2	-273.3	0.764	-357
7	12.8	-13.4	-439.4	0.764	-575
8	13.3	-6.7	-381.8	0.780	-489
9	13.3	-12.4	-385.3	0.780	-494
10	13.3	13.2	-184.9	0.780	-237
11	13.3	5.5	-244.9	0.780	-314
12	13.9	-36.4	-487.7	0.795	-613
13	13.9	-42.2	-457.0	0.795	-574
14	13.9	-42.9	-434.7	0.795	-546
15	16.1	-27.3	-420.1	0.858	-489
16	5.6	-26.6	-262.9	0.560	-469
17	6.1	-19.7	-323.4	0.575	-562
18	12.8	-6.4	-329.9	0.764	-432
19	13.9	-20.5	-366.8	0.795	-461

Table 5a. Temperature Correction Process
(Creep Runs, No Bump, Longitudinal Top, Gauge #7)

55

A	B	C	D	E	F	G
Run #	Pavement Temperature (^{0}C) T2	Lateral Distance (cm) X	Temperature Corrected Peak Strain (μe) $e_{21,x}$	$Y_{21}(X)$	CF_x^*	Temperature & Lateral Distance Corrected Peak Strain (μe) $e_{21,-10.5}$
1	41	−7.2	−332.61	−474.2	0.9090	−365.9
2	41	−6.9	−343.63	−469.0	0.8991	−382.2
3	41	−6.0	−360.17	−453.0	0.8683	−414.8
4	41	−12.4	−387.74	−538.2	1.0317	−375.8
5	42	−9.1	−346.49	−504.0	0.9662	−358.6
6	42	−12.2	−391.14	−536.9	1.0292	−380.1
7	43	−7.2	−333.55	−474.2	0.9090	−367.0

* $CF_x = Y_{21}(X) / Y(-10.5)$ where $Y(-10.5)$ for Gauge 7 = 521.69

Table 5b. Lateral Distance Correction Process
(45 km/h, Bump, Longitudinal Top, Gauge #7)

Core #	Longitudinal Top Strain Value @ -10.5 cm	* Variability Normalization Factor "CFv" Strain/ Avg Strain
0	-628.026	1.437240
1	-466.496	1.067578
2	-366.858	0.839555
3	-666.857	1.526105
4	-510.321	1.167873
5	-416.822	0.953898
6	-404.976	0.926790
7	-521.693	1.193897
8	-267.770	0.612792
9	-494.051	1.130639
10	-351.567	0.804564
11	-408.823	0.935594
12	-392.515	0.898273
13	-483.429	1.106329
14	-538.934	1.233354
15	-228.861	0.523750
Avg =	-436.967	

* Normalized strain value @ -10.5 cm divided
by average longitudinal top strain value

Core #	Longitudinal Bottom Strain Value @ -10.5 cm	* Variability Normalization Factor "CFv" Strain/ Avg Strain
0		
1		
2		
3		
4		
5		
6		
7	139.480	0.828392
8		
9	187.617	1.114288
10	307.818	1.828184
11	269.476	1.600465
12	54.983	0.326550
13	183.431	1.089424
14	84.750	0.503342
15	119.437	0.709355
** Avg =	168.374	

** LBOT0,1,2,3,4,5,6,&8 were considered bad gauges, therefore
they were excluded from the average strain value.

Table 6. Variability Correction Factors

Core Number	Strain Gauge Position (Top, Bottom) cm	Strain at Top (microstrain)	Strain at Bottom (microstrain)	Ratio of Strain Bottom / Top
0	(0.0, 13.5)	-198	91	-0.46
1	(0.0, 13.7)	-198	95	-0.48
2	(0.4, 14.4)	-191	110	-0.57
3	(1.0, 15.0)	-181	121	-0.67
4	(0.8, 14.8)	-184	117	-0.64
5	(1.3, 15.3)	-176	128	-0.73
6	(1.6, 15.6)	-171	131	-0.77
7	(1.1, 15.1)	-179	123	-0.69
8	(0.8, 14.8)	-184	117	-0.64
9	(1.7, 15.7)	-169	132	-0.78
10	(1.4, 15.4)	-174	129	-0.74
11	(1.5, 15.5)	-172	130	-0.75
12	(1.9, 15.9)	-165	134	-0.81
13	(1.7, 15.7)	-169	132	-0.78
14	(1.9, 15.9)	-165	134	-0.81
15	(2.6, 16.6)	-151	139	-0.92

Table 7. Calculated Tensile Strain at Each Strain Gauge Position

Table 8a. Wheel Force and Pavement Strain Response. 4th Axle with Bump, Top Gauges

Speed (km/h)	Load			Strain			Linear Regression	
	Mean (kN)	DLC	Max. (kN)	Mean (ue)	DSC	Max. (ue)	R^2	Slope (ue/kN)
Creep	61.075	0.037	63.470	367.3	0.056	407.760	0.0005	N/A
15	62.036	0.047	66.897	260.7	0.090	305.763	0.579	N/A
25	62.882	0.217	84.343	230.4	0.213	312.530	0.842	3.84
35	59.532	0.181	76.328	224.2	0.163	276.798	0.708	3.03
45	58.623	0.224	79.414	222.4	0.209	310.241	0.804	3.40
25-45	60.346	0.207	79.937	225.7	0.195	299.856	0.787	3.41

Table 8b. Wheel Force and Pavement Strain Response. 4th Axle No Bump, Top Gauges

Speed (km/h)	Load			Strain			Linear Regression	
	Mean (kN)	DLC	Max. (kN)	Mean (ue)	DSC	Max. (ue)	R^2	Slope (ue/kN)
Creep	61.059	0.019	63.470	425.5	0.033	449.325	N/A	N/A
15	61.862	0.016	63.683	240.1	0.058	272.638	0.004	N/A
25	63.071	0.031	65.743	241.4	0.069	272.160	0.062	N/A
35	61.069	0.059	67.398	251.3	0.067	282.632	0.002	N/A
45	59.228	0.058	64.760	249.0	0.107	296.227	0.400	N/A
25-45	61.123	0.049	65.967	247.2	0.081	283.673	0.019	N/A

Table 8c. Wheel Force and Pavement Strain Response. 4th Axle with Bump, Bottom Gauges

Speed (km/h)	Load *			Strain			Linear Regression	
	Mean (kN)	DLC	Max. (kN)	Mean (ue)	DSC	Max. (ue)	R^2	Slope (ue/kN)
Creep	62.421	0.014	63.865	143.2	0.088	161.2	0.293	N/A
15	62.915	0.021	64.620	110.6	0.104	127.397	0.135	N/A
25	62.570	0.165	76.915	99.6	0.193	125.078	0.654	1.98
35	61.245	0.089	71.893	103.5	0.116	119.100	0.615	1.66
45	60.488	0.198	79.414	103.6	0.218	135.560	0.577	1.43
25-45	61.434	0.151	76.074	102.2	0.176	126.579	0.598	1.57

Table 8d. Wheel Force and Pavement Strain Response. 4th Axle No Bump, Bottom Gauges

Speed (km/h)	Load *			Strain			Linear Regression	
	Mean (kN)	DLC	Max. (kN)	Mean (ue)	DSC	Max. (ue)	R^2	Slope (ue/kN)
Creep	61.059	0.019	63.470	173.9	0.069	196.832	N/A	N/A
15	62.855	0.020	64.558	112.9	0.098	127.838	0.077	N/A
25	62.785	0.014	64.500	109.4	0.077	120.850	0.001	N/A
35	63.678	0.043	67.176	112.6	0.088	122.850	0.016	N/A
45	59.699	0.050	63.590	113.7	0.115	132.463	0.190	N/A
25-45	62.054	0.036	65.089	111.9	0.093	125.388	0.001	N/A

* Statistics for Load of Bottom Gauges Calculated Using 8 of 16 Points

Table 8e. Wheel Force and Pavement Strain Response. 5th Axle with Bump, Top Gauges

Speed (km/h)	Load			Strain			Linear Regression	
	Mean (kN)	DLC	Max. (kN)	Mean (ue)	DSC	Max. (ue)	R^2	Slope (ue/kN)
Creep	61.018	0.026	64.010	382.4	0.044	413.415	0.0003	N/A
15	61.457	0.039	65.420	280.3	0.059	311.107	0.048	N/A
25	63.790	0.217	87.233	262.5	0.209	357.520	0.791	3.88
35	62.107	0.151	76.559	258.2	0.145	322.240	0.631	3.32
45	58.473	0.219	79.471	248.8	0.218	331.889	0.826	4.04
25-45	61.457	0.196	81.088	256.5	0.191	337.216	0.768	3.80

Table 8f. Wheel Force and Pavement Strain Response. 5th Axle No Bump, Top Gauges

Speed (km/h)	Load			Strain			Linear Regression	
	Mean (kN)	DLC	Max. (kN)	Mean (ue)	DSC	Max. (ue)	R^2	Slope (ue/kN)
Creep	63.112	0.026	66.060	443.5	0.035	473.840	N/A	N/A
15	61.511	0.024	64.715	257.3	0.043	277.563	0.025	N/A
25	62.205	0.018	64.553	261.0	0.062	290.920	0.016	N/A
35	60.258	0.071	66.342	273.9	0.067	316.265	0.096	N/A
45	57.984	0.065	64.410	267.1	0.076	291.350	0.411	N/A
25-45	60.149	0.051	65.102	267.3	0.068	299.512	0.110	N/A

Table 8g. Wheel Force and Pavement Strain Response. 5th Axle with Bump, Bottom Gauges

Speed (km/h)	Load *			Strain			Linear Regression	
	Mean (kN)	DLC	Max. (kN)	Mean (ue)	DSC	Max. (ue)	R^2	Slope (ue/kN)
Creep	61.462	0.027	64.010	155.3	0.143	192.935	0.0014	N/A
15	61.979	0.035	65.087	115.9	0.123	140.320	0.114	N/A
25	59.463	0.183	78.767	105.3	0.217	146.129	0.620	1.760
35	63.851	0.145	76.559	117.8	0.148	154.374	0.380	N/A
45	55.786	0.200	78.981	103.5	0.199	135.744	0.445	N/A
25-45	59.700	0.176	78.102	108.9	0.188	145.416	0.507	1.38

Table 8h. Wheel Force and Pavement Strain Response. 5th Axle No Bump, Bottom Gauges

Speed (km/h)	Load *			Strain			Linear Regression	
	Mean (kN)	DLC	Max. (kN)	Mean (ue)	DSC	Max. (ue)	R^2	Slope (ue/kN)
Creep	63.112	0.026	66.060	173.9	0.100	211.642	N/A	N/A
15	62.132	0.027	64.715	117.7	0.073	131.363	0.0001	N/A
25	62.424	0.017	64.500	110.9	0.096	131.048	0.015	N/A
35	61.928	0.058	66.732	119.6	0.100	134.166	0.176	N/A
45	58.876	0.060	64.410	123.4	0.143	149.573	0.275	N/A
25-45	61.076	0.045	65.214	118.0	0.113	138.262	0.060	N/A

* Statistics for Load of Bottom Gauges Calculated Using 8 of 16 Points

60

REFERENCES

1. Kenis, W.J., and Rhode, G., 'Primary Response under Heavy Truck Traffic.' Proc. 7th Int. Conf. on Asphalt Pavements, Vol. 2, pp 201-215, 1992.

2. ARE Inc., Impact of Truck Characteristics on Pavements: Truck Load Equivalency Factors, U.S. Department of Transportation, Federal Highway Administration, FHWA-RD-91-064, July 1992.

3. Kenis, W.J., 'Dynamic Load Effects on Pavement Primary Response and Future Research.' Dynamic Loading of Heavy Vehicles and Road Wear Mid-Term Seminar, Paper 11, pp 1-21, February 1995.

4. Newland, D.E. Random Vibrations and Spectral Analysis , 2nd edition , Longman,1987.

5. Sweatman, P. F., A Study of Dynamic Wheel Forces In Axle Group Suspensions of Heavy Vehicles, Australian Road Research Board, Special Report No 27, 1983.

6. Cebon, D., 'An Investigation of the Dynamic Interaction Between Wheeled Vehicles and Road Surfaces.' PhD Thesis, University of Cambridge, 1985.

7. Hammouda, J., 'Critical Strain Response to Dynamic Moving Load.' Technical Documents, EBA Engineering, 1997.

Reproduced by NTIS

National Technical Information Service
Springfield, VA 22161

This report was printed specifically for your order
from nearly 3 million titles available in our collection.

For economy and efficiency, NTIS does not maintain stock of its vast collection of technical reports. Rather, most documents are printed for each order. Documents that are not in electronic format are reproduced from master archival copies and are the best possible reproductions available. If you have any questions concerning this document or any order you have placed with NTIS, please call our Customer Service Department at (703) 487-4660.

About NTIS

NTIS collects scientific, technical, engineering, and business related information — then organizes, maintains, and disseminates that information in a variety of formats — from microfiche to online services. The NTIS collection of nearly 3 million titles includes reports describing research conducted or sponsored by federal agencies and their contractors; statistical and business information; U.S. military publications; audiovisual products; computer software and electronic databases developed by federal agencies; training tools; and technical reports prepared by research organizations worldwide. Approximately 100,000 *new* titles are added and indexed into the NTIS collection annually.

For more information about NTIS products and services, call NTIS at (703) 487-4650 and request the free *NTIS Catalog of Products and Services*, PR-827LPG, or visit the NTIS Web site **http://www.ntis.gov**.

NTIS
Your indispensable resource for government-sponsored information—U.S. and worldwide

U.S. DEPARTMENT OF COMMERCE
Technology Administration
National Technical Information Service
Springfield, VA 22161   (703) 487-4650